AD-A212 109

UNCLASSIFIED
SECURITY CLASSIFICATION OF THIS PAGE

(2)

REPORT DOCUMENTATION PAGE

Form Approved OMB No. 0704-0188

1a. REPORT SECURITY CLASSIFICATION: UNCLASSIFIED	1b. RESTRICTIVE MARKINGS: DTIC FILE COPY
2a. SECURITY CLASSIFICATION AUTHORITY: SEP 11 1989 E	3. DISTRIBUTION/AVAILABILITY OF REPORT: APPROVED FOR PUBLIC RELEASE DISTRIBUTION IS UNLIMITED
2b. DECLASSIFICATION/DOWNGRADING SCHEDULE	
4. PERFORMING ORGANIZATION REPORT NUMBER(S)	5. MONITORING ORGANIZATION REPORT NUMBER(S): AFOSR-TR- 89-1210
6a. NAME OF PERFORMING ORGANIZATION: STANFOR UNIV	6b. OFFICE SYMBOL (If applicable):
6c. ADDRESS (City, State, and ZIP Code): MECHANICAL ENGINEERING STANFOR, CA 94305	7a. NAME OF MONITORING ORGANIZATION: AFOSR/NA
	7b. ADDRESS (City, State, and ZIP Code): BUILDING 410 BOLLING AFB, DC 20332-6448
8a. NAME OF FUNDING/SPONSORING ORGANIZATION: AFOSR	8b. OFFICE SYMBOL (If applicable): NA
	9. PROCUREMENT INSTRUMENT IDENTIFICATION NUMBER: AFOSR-86-0159
8c. ADDRESS (City, State, and ZIP Code): BUILDING 410 BOLLING AFB, DC 20332-6448	10. SOURCE OF FUNDING NUMBERS: PROGRAM ELEMENT NO. 61102F; PROJECT NO. 2307; TASK NO. A3; WORK UNIT ACCESSION NO.
11. TITLE (Include Security Classification): (U) ACTIVE CONTROL OF UNSTEADY AND SEPARATED FLOW STRUCTURES	
12. PERSONAL AUTHOR(S): J. EATON, D. KOGA	
13a. TYPE OF REPORT: FINAL REPORT	13b. TIME COVERED: FROM Apr 15 86 TO Apr 14 89
14. DATE OF REPORT (Year, Month, Day): MAY 1989	15. PAGE COUNT: 60
16. SUPPLEMENTARY NOTATION	

17. COSATI CODES		
FIELD	GROUP	SUB-GROUP

18. SUBJECT TERMS (Continue on reverse if necessary and identify by block number): UNSTEADY FLOWS, FLOW CONTROL, [illegible]

19. ABSTRACT (Continue on reverse if necessary and identify by block number)

The objective of the research program was to formulate an active flow control method to change the vorticity and convection characteristics of a modelled dynamic stall vortex. Flow visualization, surface pressure and laser doppler anemometer measurements were obtained. A potential flow model was developed as a state estimator and several flow control strategies were examined.

Keywords: Aerodynamic Stability, [illegible]

20. DISTRIBUTION/AVAILABILITY OF ABSTRACT: ☐ UNCLASSIFIED/UNLIMITED ☒ SAME AS RPT. ☐ DTIC USERS	21. ABSTRACT SECURITY CLASSIFICATION: UNCLASSIFIED
22a. NAME OF RESPONSIBLE INDIVIDUAL: HENRY E. HELIN	22b. TELEPHONE (Include Area Code): 202-767-0471 / 22c. OFFICE SYMBOL: AFOSR/NA

DD Form 1473, JUN 86 — Previous editions are obsolete. — SECURITY CLASSIFICATION OF THIS PAGE: UNCLASSIFIED

Final Technical Report

Grant No. AFOSR-86-0159

for the three-year period ending April 14, 1989

AIR FORCE OFFICE OF SCIENTIFIC RESEARCH

ACTIVE CONTROL OF UNSTEADY AND SEPARATED FLOW STRUCTURES

Principal Investigator: John K. Eaton

Associate Investigator: Dennis J. Koga

Thermosciences Division
Department of Mechanical Engineering
School of Engineering
Stanford University
Stanford, California 94305

May 1989

ABSTRACT

This document summarizes the Air Force Office of Scientific Research Grant No. AFOSR-85-0159 entitled "Active Control of Unsteady and Separated Flow Structures". The objective of the research program was to formulate an active flow control method which was capable of changing the vorticity and convection characteristics of a modelled dynamic stall-type vortex.

The modelled unsteady, spanwise, separated flow vortex was generated using a computer-controlled, flush-mounted flap (or spoiler) over a range of sinusoidal and variable duty cycle triangle waveform motions. The effective reduced frequency range was 0.025 to 0.10 and included oscillatory, one-shot and pitch-and-hold motions.

Phase-conditioned flow visualization, surface pressure and laser Doppler anemometry measurements were obtained, and the processed velocity vectors and vorticity contour development were reconstructed into animated computer movies. From these results, the dominant vorticity transport mechanism of the vortex development was found to be inviscid, accounting for over 80% of the transport energies, as long as the vortex could be readily identified by closed vorticity contours.

Based on this inviscid transport mechanism, a potential flow model was successfully implemented to act as a real-time flow state-estimator using surface pressure time signatures at nine different streamwise locations. In addition, a discrete-vortex model code was formulated to model the time-developing vortex flow over the flap, and to act as a control loop plant model. However due to computational speed restrictions of the present hardware, this plant model could not be implemented in a real-time algorithm.

Several vortex control experiments were performed using different vorticity flux modification strategies. It was found that upstream three-dimensional flow structures were ineffective due to the sharp-edged separation of the flap used to create the large separation vortex. Also, once the vortex has formed and is convecting, downstream flow control devices are ineffective except for reducing surface pressures by displacing the vortex away from the surface.

When two-dimensional, upstream, spanwise blowing or a secondary, smaller spanwise flap was utilized to alter the approach flow boundary layer vorticity flux, successful modification of the large separation vortex was achieved. Vortex convection delays in the range of ± 25 degrees of the effective flap cycle and a vortex suction peak amplitude control of up to 40% were achievable.

These manual open loop control experiments were performed over a wide parameter range space, and appropriate control conditions, such as control flap speed and phasing, were identified for use in an optimized closed-loop control experiment. Preliminary experiments have analyzed specific control parameters such as actuator time delay and sensor response, and an active control loop experiment is in progress. This experiment will entail the fast detection of the forming vortex using surface pressure measurements and feedback from the inviscid vortex state-estimator algorithm in an effort to control the vortex convection and suction peak behaviors according to pre-programmed limits. The results of this work will be detailed in the AFOSR-DoD Flow Control URI Final Report from Stanford University, expected October 1989.

TABLE OF CONTENTS

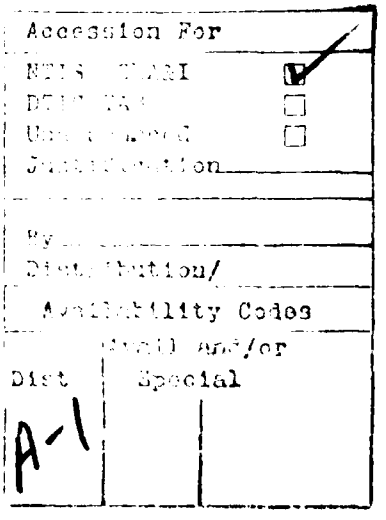

INTRODUCTION AND OBJECTIVES

In the past few years, new research goals have focused on the possibilities for post-stall flight and aircraft supermaneuverability. The tactical advantages of aircraft supermaneuverability have been well established by Herbst [1983], and additional safety advantages are quite apparent for aircraft with a reasonable degree of post-stall maneuvering capabilities. Current research efforts directed towards achieving such goals of post-stall flow control encompass a wide range of programs from experiments that study the characteristics of the unsteadiness associated with flow separation to the latest experiments that attempt to alter the characteristics of the unsteady, separated flowfield.

Introduction

The solution to the problem of post-stall maneuverability involves the control of flow in two quite different flow regimes. As the aircraft initially exceeds the static stall angle, the phenomenon of dynamic stall becomes important, particularly in fast-accelerating aircraft motions. At this point, the airfoil can exceed its maximum steady-lift coefficient by more than a factor of two, due to the temporary presence of a large spanwise, leading edge vortex. However for sustained post-stall maneuverability, upper-surface airfoil flow control must be maintained as the dynamic stall-stall vortex sheds off the surface and the flow adjusts to the steady, separated-flow regime. Additionally, it will be necessary in most cases to modify the steady, separated flowfield in order to maintain adequate lift.

Historically, the unsteady and separated-flow processes have most often been investigated using oscillating airfoil experiments in dynamic stall. McCroskey *et al.* [1975] established the time-history development of the unsteady, high-lift characteristics of the leading-edge vortex before the catastrophic flow-separation process, and Carr *et al.* [1977] identified various types of mechanisms leading to dynamic stall. The identification of these mechanisms, which include trailing-edge stall and boundary layer flow reversal, bursting of the leading-edge separation bubble, and separation of the turbulent boundary layer, will be vital for the eventual consideration of dynamic-stall control.

Research in both the physics of the dynamic stall process and its control has accelerated in recent years with the hope of capturing these advantages. Several investigators including Helin [1986], Albertson, *et al.* [1987], and Walker and Chou [1987], have utilized modern measurement techniques to gain new insights toward the understanding of the vorticity roll-up mechanisms of the dynamic stall process on the oscillating airfoil. Recent results have shown that pitch-motions (in addition to just pitch rates) and leading-edge slats have significant effects on dynamic stall vortex growth rates. Also of significance is the conclusion that the high-lift of the dynamic stall process is not associated with the large dynamic stall vortex, but rather with the earlier stage large vorticity production which feeds the dynamic stall vortex.

Some examples of current flow modification experiments, applicable to dynamic stall flowfields, include the work of Freymuth, *et al.* [1988] which showed that flow can be held attached to an airfoil pitching from 0 to 40 degrees through the use of a high-speed rotating leading edge nose on the airfoil. Luttges, *et al.* [1985] utilized an oscillating airfoil with moveable vortex generators or pulsed air injection which demonstrated some sensitivity of vortex formation and shedding phase to external

manipulators. Huang, *et al.* [1987] utilized an airfoil with sound excitation near the leading edge and were able to significantly increase the static stall angle. Shih, *et al.* [1987] employed an oscillating flap installed on an airfoil in an oscillating freestream and realized a significant reduction in the size of the separation zone; similar to the steady separation results of Koga [1983] and Reisenthel [1984] using a flap on a flat plate wedge and backstep flow separations, and Francis, *et al.* [1979] using an oscillating fence-type spoiler on an airfoil.

Other investigations have been aimed at the interaction of flow structures for control purposes in more generic flow configurations. Wygnanski, *et al.* [1988] utilized a wall jet, Acharya [1987] a spanwise blowing slot on a flat plate, Chow and Sheen [1987] a free vortex interacting with an oscillating airfoil, and Viets and Ball [1981] a rotor imbedded in the wall. The common principle among all these investigations is the technique of modifying the wall layer vorticity flux, as discussed in detail by Reynolds and Carr [1988].

Objectives

In order to accomplish the objective of modelled dynamic-stall type vortex control, the research program was divided into three main phases. A detailed description of each part of the three-phase research program has been described by Koga, *et al.* [1987].

Summarizing briefly, in the first phase, detailed measurements were made to obtain a basic understanding of the vorticity formation and evolution of the dynamic-stall modelled vortex. These details would be necessary for the proper planning of a control stategies and state estimators for the vortex dominated flowfield. The second phase work was designed to establish vortex state detection criteria and the development of a simple vortex state estimator model based on the first phase analyses of the modelled vortex behavior. This model would be utilized in the last stages of the third phase in an effort to construct a closed-loop control scheme. Additional preliminary work in the third phase would be needed to determine the proper actuator methods for effective modification of the modelled dynamic stall flowfield.

EXPERIMENTAL FACILTIES AND TECHNIQUES

The research program was carried out in two main wind tunnel facilities at Stanford University. The first facility is a 15 cm x 45 cm cross-section test section wind tunnel called HMT-1 and described in some detail by Nelson, *et al.* [1989-a]. This facility is the primary facility used for all experimental work except the two-flap experiments discussed later. HMT-1 is equipped with a traversable single-component, rotatable LDA system and a Masscomp MC-5500 data acquisition system. In addition, the test section was also fully instrumented for smoke-wire flow visualization, surface pressure measurements and hot-wire boundary layer traversing.

Special data handling techniques for phase-bin processing of the random arrival times of the acquired LDA data samples and the subsequent reconstruction of the two-dimensional, phase-averaged velocity and vorticity fields have been discussed by Nelson, *et al.* [1989-a and 1989-b].

Due to a moderate degree of wind tunnel confinement effects experienced in the HMT-1 facility, a second and larger scale flow-control wind tunnel facility was completed during the course of this research program. This facility has been used for latter research phase control experiments which allowed larger flap lengths and lower frequencies to be utilized. This new, closed-return wind tunnel has a larger (0.9 m. x 0.6 m. x 3.75 m.) fully transparent test section and is capable of a maximum test section speed of 25 m/s. Benchmark data has shown the freestream flow in the test section to be uniform within 2% and exhibit less than 0.05% freestream turbulence at approximately 10 m/s flow speeds. A splitter plate with a dual low blockage flap mechanism was installed in the test section. The plate was equipped with smoke-wire flow visualization and surface pressure measurement capabilities, in addition to a full length two-dimensional hot-wire probe traversing mechanism.

The flow-control wind tunnel and the dual-flap system are computer controlled by a Masscomp MC-5520 system, which also acquires all pressure and velocity data signals. An additional PDP-11/23 system was available for use as the real-time control loop feedback acquisition and processor slave.

RESEARCH PROGRAM RESULTS

The overall experimental plan and some preliminary results have been described by Eaton, *et al.* [1988] and Koga, *et al.* [1987]. In summary, the purpose of this work was to identify successful methods of modifying the formation, growth and release of a simplified dynamic stall type vortex, which would then allow construction of a working closed-loop active control experiment using fast flow detection and flow state estimation. A flush mounted flap (acting as a spoiler) was utilized to generate a strong and coherent spanwise vortical flow element which served as the simplified dynamic stall vortex model. The controllable flap allowed the generation of periodic spanwise vortices with a useful reduced frequency range between 0.025 and 0.10, and also had the capability of generating pitch-and-hold motions.

Mechanisms for Spanwise Vorticity Transport

The phase-development of the oscillating flap unsteady vortex flow has been documented using smoke-wire flow visualization, surface pressure measurements and two-component LDA velocity mapping at several flap reduced frequencies. The cyclic phase-developing vorticity field was then computed for the various flap oscillation frequencies and also a pitch-and-hold flap motion. Typical field results are shown in Figures 1 and 2. More complete data cycles were presented in Nelson, *et al* [1989-a and 1989-b], copies of which are included in Appendix B. The velocity, vorticity and pressure fields have been superposed in the form of a phase-developing animated color movie, displayable on the Masscomp computer systems.

The first research phase investigated the physics of the developing unsteady, separated flow vortex behind an oscillating flap (the modelled dynamic stall type vortex). Significant results from this research phase were presented by Nelson, *et al.* [1987]. In summary, it was determined that the viscous and turbulent diffusion terms of the governing vorticity transport equation were not significant for this class of unsteady, separating flows (sinusoidal flap motions in the reduced frequency range where distinct vortex structures are produced). This established the predominant non-linear convective behavior of the model dynamic stall vortex. It was thus concluded that a simple inviscid flow model for the first-order unsteady vortex state estimator was practical. This utilization has been verified by accurate vortex state sensing with simple (nine spatial data point profile) surface pressure measurements mathematically fitted to an inviscid Rankine-type vortex model as shown by Nelson, *et al.* [1989-a]. The modelling features will be discussed further in a later section.

Vortex Control Experiments

The control of the developing vortical flow region behind the pitching flap has been based on steady separation control and vortex development documentation of Koga [1983] and Reisenthel [1984]. A simplified overview of the vorticity interactions involved in this steady separation control has been proposed by Reynolds and Carr [1985]. This concept of vorticity flux management is vital to flow control attempts. The control premise has been that by upstream (or close downstream) modulation of the vorticity flux into (or out of) the developing separated flow region, the overall phase behavior and shedding characteristics of the modelled dynamic stall vortex may be proportionally controlled by regulation of the local vorticity "accumulation" into a large, strong vortex structure.

(a) Three-dimensional Vortex Elements

As discussed by Nelson, *et al.* [1989-b], several attempts at modifying the formation of the vortical structure were performed, including the introduction of two and three-dimensional disturbances upstream of, and at the flow separation point. Longitudinal vortex generators and small three-dimensional disturbances had little effect on the forming separated flow region; in retrospect due primarily to the sharp-edged (and thus fixed separation line) characteristic of the pitching flap. Small amplitude modulation of the pitching flap itself did show a slight effect on the separated region vorticity by providing an unsteady pumping-type release of small amounts of vorticity. However the overall formation time and strength of the separated flow region were not significantly altered, although the steady reattachment length was decreased markedly.

(b) Two-dimensional Pulsed Blowing

Promising results were achieved utilizing pulsed blowing (from an acoustic speaker) through an angled, spanwise slot located upstream of the flap, as illustrated in Figure 3. In this control experiment, both the flow-separating flap and the speaker blowing were 8 Hz sinusoidal oscillations, with the phase differential between the waveforms and the blowing amplitude as parameters. Full streamwise surface-pressure profiles were recorded, and the downstream point of $x/L=3$ was chosen as a criterion point for the following results. The phase-varying surface pressure measurements of Figure 4 and the smoke-wire photographs of Figure 5 documented how the pulsed blowing successfully modulated the vorticity flux upstream of the flap so that the accumulation and resultant shedding of vorticity in the primary separated flow vortex could be phase-delayed.

In Figure 4, a phase-development variation of nearly 25 degrees (between the low pressure valleys, relative to the flap motion) was achieved by varying the relative phase angle between the blowing waveform and the flap waveform. It should be noted that the speaker actually produces alternating blowing/suction cycles, which explains the slight phase lead in the zero degree speaker lag waveform of Figure 4.

As seen in the visualization records of Figure 5, the mechanism for the observed surface pressure phase delay is more apparent. When the proper relative blowing phase is utilized, the pulsed flow out of the slot acts to roll-up the oncoming vorticity flux into a small vortical structure upstream of the flow-separating flap. This effectively produces a local "stalling" of the normal vorticity flux to the separated shear layer and thereby phase-retards the accumulation of vorticity, roll-up and subsequent vortex shedding from the flap.

A rather surprising result appeared in the blowing input power parameter investigations, as shown in Figure 6. It is clear that both the mean surface pressures and the vortex phase-delay functions can be related to the speaker input power variable using simple empirical relations. In terms of controllability of the flow, this means that the flow actuator model can be represented by a relatively simple, monotonic mathematical relation, which will aid significantly in the formulation of a closed-loop control experiment by allowing stable proportional control inputs.

In the case of the pitch-and-hold flap motion (actually a 1 Hz periodic waveform with the flap rising in an 8 Hz equivalent motion, then holding), when the speaker is pulsed at a frequency of 8 Hz the cyclic pressure-phase plot of Figure 7 is obtained.

Many different speaker waveform phase lags were examined, and several are plotted here. Note that a 45 degree speaker phase lag (relative to the flap waveform) is equivalent to one full speaker cycle shift (since 1/8 cycle = 45 degrees). The most significant results in Figure 7 are first that the transient, interactive pressure response of the separating flap flow field to the speaker pulsing is limited to about one full speaker cycle (45 flap phase degrees). Secondly, the subsequent flap phases are a relatively straight-forward superposition of the pulsed-flow vortices on top of the separating flow region. An additional interesting observation was that pulsed-flow vortices were amplified by a factor of about four by the separated flow shear layer (as indicated in the oscillation amplitudes from flap phases 45-225 degrees when the flap is near its highest point, compared to flap phases 270-345 degrees when the flap is nearly flat on the plate). This natural amplification will be an important consideration in determining control input magnitudes and rates for possible future steady separation buffet control applications.

In order to more accurately determine the transient effects of the pulsed-blowing on the pitch-and-hold flap flowfield, the first 90 degrees of flap phase have been expanded in Figure 8. It is quite evident that the convecting vortex structure, indicated by the low pressure peaks, has been phase-delayed for approximately 15 degrees of flap phase (from 20 degrees flap phase to about 35) when the speaker phase waveform lags the flap by 40 degrees. This also appears to be true over a significant range of the vortex generating flap reduced frequencies, so that the actual time (rather than phase) delays can be quite significant for low effective reduced frequencies of the flap.

(c) Dual-flap Configuration

Vortex modification experiments have been performed in the new, large-scale flow control wind tunnel using a dual-flap configuration. As shown in Figure 9, the primary flap is 5 cm. in height and is used to generate the spanwise, separated flow vortex which is the dynamic-stall vortex model. In addition, a second flap (1.5 cm. in height) is used as the control device. The smaller size of the control flap was chosen to be more representative of the scale of actuator to flow-structure sizes reasonable for flow scenarios like the dynamic stall case. The control flap has been located either 10 cm. upstream or downstream from the primary vortex generating flap and primary dynamic-stall type vortex structures were generated using either one-shot or lift-and-hold flap motions in the following studies. The primary parameter space investigated for the dual-flap experiments were: (i) control to separating flow flap frequency ratios of 1.0, 2.0 and 3.0, (ii) flap motion limits from 0 to 90 degrees, (iii) control to separating flow phase delays from -180.0 to 360.0 degrees relative to the stall flap motions, (iv) sinusoidal and a wide range of ramp-type flap motions, (v) one-shot control motions versus continuous flap motion, triggered at the specified phase delay, and (vi) phase-conditioned surface pressure measurements made at three downstream locations as shown in Figure 9.

For the case where the control flap was located downstream of the primary vortex generation point, Figure 10 shows that while there were no significant phase/time delay effects on the convecting vortex, the primary suction peaks could reduced by significant amounts. Interpretation of this result showed that once the primary vortex was formed and convecting, no significant vorticity control could be exercised on the vortex with the available reduced control flap size. The reduction in the primary suction ($-C_p$) peak value is attributed to a simple lifting of the vortex away from the surface, thereby reducing the magnitudes of the negative pressures on the surface. The secondary suction peaks for the early control delay values are simply the premature arrival of the control vortex structure at the measurement station. (Note:

design limitations of the flap drive mechanisms prohibited the placement of the control flap within the vortex formation region, *i.e.* the first flap height downstream, of the primary stall vortex where actual interference with the shear layer roll-up would have been possible. This lack of close positioning was not considered detrimental since this would have produced unrealistically small control actuation time limits for the later stage active control experiments.

More effective control was obtained by implementing the smaller control flap upstream of the primary separating flow flap, and the following discussion will deal exclusively with this geometry. The mechanism for the upstream control flap is similar to the pulsed blowing work, wherein the approach flow boundary layer vorticity is rolled-up into small vortices which tend to discretize the vorticity flux and thus produce some phase control of the vorticity reaching the separating flow flap tip. Note however that this flap case does not produce opposite-signed vorticity as in the case of the pulsed blowing/suction cycle of the speaker.

Figure 11 shows an example of the range of phase control possible with the dual-flap experiments. The surface pressure signatures at three different downstream locations are plotted for a wide range of control flap phase delays (referenced to the stall flap motion). It is evident that the arrival of the primary vortex can be somewhat shifted in phase, usually accompanied by a suction peak pressure change. This phase shift can be noted either by a shift in phase of the suction peak or the displacement of the rapid pressure drop-off which is characteristic of the "arrival" of the stall vortex.

Over most of the wide parameter range tested, the greatest control effects were obtained when the control flap motion occured at twice the frequency of the stall flap. It is also evident from Figure 11 that by x/H=5.0, the primary vortex has experienced significant viscous interaction with the test plate surface, creating a leading rise in the pressure signature. In order to avoid this increased pressure effect, the rest of the results will be discussed at x/H=2.5, where a "clean" pressure signature is readily obtainable.

The first parametric studies were done with sine wave motions for both the stall and control flaps. Figure 12 shows summary plots of the control effect on the vortex convection delay (expressed in terms of a phase shift) and also on the resulting change in the peak suction pressures, for these continuous flap motions. There are conditions wherein both vortex delay and suction peak amplification could be achieved (control flap phasing from about 60 to 160 degrees ahead of the stall flap). This combined augmentation effect was seen only in the continuous flap motion cases. For the more realistic cases of single stall vortex motions, a phase delay of the convecting vortex resulted in an attenuation of the suction peak. The following discussions will now concentrate on phase-delays rather than phase-advancing, due to their more convenient application into a control loop strategy which is already limited by very short time restrictions.

As a note, it was observed in the parametric surveys that in many of the successful primary vortex convection phase delay experiments, control needed to activated before the stall flap motion began, which is not practical for a reactive flow control scenario. However this knowledge can still be beneficial for enhancing pre-programmed flight maneuvers. In addition, the cases which provide phase-advancing could also be useful for causing premature shedding of the primary vortex structures which may be critical in keeping roll-moments on the aircraft to a minimum by simultaneously shedding vortices off each wing.

Figure 13 shows mean surface pressure signatures for pitch and hold flap motions which generate a separated flow vortex that convects downstream leaving a large separated flow region. Due to the non-continuous nature of the pitch and hold motion, the delay in vortex arrival at the measurement station is described by an effective non-dimensional cycle time. Delays up to 0.2 cycles (or about 40 msec) for the effective 5.0 Hz stall flap motion were observed. It should be noted that this enhanced delay time can be attributed to the slower convection speed of the vortex as it smears its vorticity throughout the separation downstream of the flap, now held at its maximum actuation angle.

In order to generate and maintain a single, clean primary spanwise vortex, one-shot flap motions were used. Figure 14 shows the clean pressure recovery of the mean pressure signatures for the one-shot stall flap motions. For this case, the range of control effectiveness is about 40% in suction pressure peak, and $\pm$20 degrees in vortex convection phase delay as shown in Figure 15. Again note that there is a significant range of control actuation lag time (0 to 60 degrees) available which still allows effective vortex convection control, although the vortex suction peak can only be attenuated in this lag time range.

It should also be noted that triggered control (wherein the control flap starts at a given phase delay, but remains oscillating) produces similar results to the one-shot cases, only with additional secondary suction peaks merely superimposed on the mean pressure signatures. The only exception to this superposition effect was the pitch and hold stall flap motions wherein late control vortices were amplified in the held flap shear layer region.

Since it was desirable to provide the maximum control actuation lag time for a successful control loop implementation, triangle waveform one-shot flap motions were utilized to increase the phase delay effectiveness of the vorticity roll-up mechanism in the separated flow vortex. In particular, utilizing a slowly rising (90% of the cycle, designated T90) and fast falling stall flap was expected to significantly increase the available control interval from the detection to the actuation stage. Figure 16 shows results of the control tests on the T90 triangle waveform stall flap motions, for a range of control flap waveform motions. Figure 16(a) shows that a slow-rising control flap doesn't significantly delay the vortex arrival although it does attenuate the suction peak. The T50 control flap motion of Figure 16(b) is effective in producing a shift in the vortex convection time with minimal attenuation of the suction peak. It should be noted that this T50 waveform produces equivalent results to a pure sinewave control motion waveform, which will be useful in minimizing the complexity of a control loop formulation.

Vortex Detection and Modelling

Based on the inviscid dominance result of the spanwise vorticity transport mechanism studies, effort was concentrated on the development of a computational discrete vortex model for flow prediction and flow state estimation. Basic discrete vortex element methods summarized by Spalart [1988] were utilized in a time-developing code which incorporated special handling of the moving flap boundary conditions for vorticity blob creation. The vorticity shedding from the flap tip was modelled by introducing finite vorticity blobs of strength proportional to the boundary layer profile velocity past the flap tip and on a trajectory tangent to the flap angle. These criteria were found to adequately represent the vorticity flux fed into the shear layer created by the moving flap.

In order to adequately scale the necessary time steps for the flap shedding, 60 vortex blobs per flap cycle were implemented. These model specifications could not be run at real-time speeds for the flow velocities used and the present Masscomp computer hardware configuration. However it was estimated that with available special floating point processors and some improvement in vorticity blob merging algorithms, this speed problem may be overcome in the future.

It was also hoped that the present discrete vortex model could be utilized in numerical vorticity interaction studies such as the dual-flap scenario case. However the special (and artificial) handling of the flap shedding for creation of the vorticity blobs did not allow this capability. However recent independent work by Ghia, *et al.* [1989] and also by Chawla and Chow [1989] provides hope for an adequate model which can handle the difficult moving boundary condition problems that flaps and spoilers present. These works should provide the capability for future numerical experiments, although their computationally intensive nature will preclude their use as real-time flow-state estimators.

In terms of control application, it is evident that a traditional discrete vortex method is inadequate in terms of present day computational speed. However away from the very early stages of the vorticity sheet roll-up, the formed vortex characteristics can be accurately estimated by a few surface pressure measurements and a simple inviscid vortex model as shown by Nelson, *et al.* [1989-b]. This basic model for the flow state estimator allows real-time speed calculations and is designed to be used in conjunction with a digital predictor/corrector algorithm in an active flow control loop.

Active Flow Control Experiment

The vortex control experiments have shown that a significant degree of modification can be made on the modelled dynamic stall vortex by upstream vorticity flux regulation. These experiments themselves were actually a kind of open-loop control performed with the investigators acting as the "feedback" to narrow down the parameter space. These open-loop control results have shown that for the "best case" control actuator application, whether it was spanwise-blowing or a second mechanical flap configuration, a phase delay of approximately 25 degrees, which corresponds to 14 ms at 5 m/s, or 35 ms at 2 m/s freestream speeds, could be achieved for the same effective reduced frequency consideration. In addition, a pressure peak attenuation of 40% or amplification of 20% could also be generated by the appropriate modification of the stall vortex flow structure.

In order to realize the above vortex control, the actuator needed to be lagging the stall flap motion by about 0.125 cycles or 45 phase degrees, which translated to a mere 25 msec for the low condition of 5 m/s freestream velocity. This very small sensing and actuator lag would cause serious control loop design limitations.

In order to complete the present program work in implementing a true flow control loop scheme, a case where successful control could be applied and which also provided a reasonable amount of actuator lag time needed to be defined. In order to meet the latter criterion, it was decided to utilize the lower 2 m/s freestream velocity condition. Figure 17 shows that the vortex control effects of convection phase delay are maintained at this lower speed. The delay characteristic avalivable for this model case is a 75 msec (0.15 cycle time for the effective 2 Hz motion) vortex convection delay when the control flap is actuated about 125 msec (0.25 cycle time) after the stall flap one-shot

initiation. This will be the design criteria for the active control loop experiment. It should be noted that once the actual control loop is established, it is expected that effective control should be realizable over a much wider range due to the control feedback nature. The above limits were established only to give design guidelines and feasability for the control loop construction.

The remaining speed questions are whether the sensing, calculations and control flap actuator are fast enough to meet the above time restriction. Figure 18 shows the time response of the control flap actuator system relative to its input control signal. For the range of conditions necessary for generation of the control vortices, the control flap inertial lag is estimated to be about 9 msecs, with the sensing of pressure taking an additional 1 or 2 msecs.

A more limiting time constraint turned out to be the Unix based Masscomp computer system which has unpredictable (and quite long) response delays. Figure 19 shows the result of an experiment wherein the Masscomp was programmed to return a control signal output from its D/A converter, triggered at an arbitrary time by a threshold value of an A/D line that it monitored. The large range of response times are a direct result of the unresponsive Unix environment. In order to overcome this computer limitation, a more real-time response computer, a PDP-11/23, is being implemented which should provide predictable and repetitive loop times on the order of 10 msec.

An additional criterion in the control loop scheme is the definition of a state estimator. Present results have shown that a simple inviscid vortex model plant is adequate and surface pressure measurements monitoring the suction pressure and its time-slope are expected to be adequate for updating the model plant. The construction of this real-time, active control loop experiment is currently in progress, supported as part of this Grant No. AFOSR-85-0159 which was transferred to the AFOSR-DoD Flow Control University Research Initiative (URI) award to Stanford University. The final results of this work will be reported at the conclusion of the URI in October 1989.

ACKNOWLEDGEMENTS

Research assistance for this AFOSR-85-0159 grant has been provided by one Ph.D. candidate, Mr. Curtis F. Nelson, and one Masters degree student, Mr. Edwin Y. Noma. A Ph.D. dissertation with a more detailed discussion of results will be completed by Mr. Nelson in the near future.

Additional model fabrication assistance has been provided by Mr. Robin Birch and his staff of the Thermosciences Division shop in the Mechanical Engineering Department at Stanford University.

REFERENCES

Acharya, M. [1987], "Investigation of Reactive Control of Separated Flows with Non-stationary Separation Lines," Proceedings of the AFOSR Unsteady Separated Flow Workshop II, Colorado Springs, CO, July 28-30.

Albertson, J.A., Troutt, T.R., Siuru, W.D. and Walker, J.M. [1987], "Dynamic Stall Vortex Development and the Surface Pressure Field of a Pitching Airfoil," Paper AIAA-87-1333, AIAA 19th Fluid Dynamics, Plasma Dynamics and Lasers Conference, Honolulu, HI, June 8-10.

Bhattacharjee, S., Scheelke, B. and Troutt, T.R. [1985], "Modification of Vortex Interactions in a Reattaching Separated Flow," Paper No. AIAA-85-0555, AIAA Shear Flow Control Conference, Boulder, CO, March 12-14.

Carr, L.W., McAlister, K.W. and McCroskey, W.J. [1977], "Analysis of the Development of Dynamic Stall Based on Oscillating Airfoil Experiments," NASA TN-8382, Jan.

Chawla, K. and Chow, C. [1989], "Vortical Flows Past Normal Plate and Spoiler of Time Dependent Height," Paper No. AIAA-89-0291, AIAA 27th Aerospace Sciences Meeting, Reno, NV, January 9-12.

Chow, C.Y. and Sheen, Q.Y. [1987], "Unsteady Vortical Flows Around Airfoil," Proceedings of the AFOSR Unsteady Separated Flow Workshop II, Colorado Springs, CO, July 28-30.

Eaton, J.K., Jeans, A.H., Ashjee, J. and Johnston, J.P. [1979], "A Wall-Flow-Direction Probe for Use in Separating and Reattaching Flows," J. Fluids Engrg., **101**, pp.364-366.

Eaton, J.K., Johnston, J.P. and Koga, D.J., [1988], "Active Control of Separating and Fully Separated Flows", Research on Turbulence: AFOSR Contractors' Meeting, Los Angeles, CA, June 28-30.

Francis, M.S., Keesee, J.E., Lang, J.D., Sparks, G.W. and Sisson, G.E. [1979], "Aerodynamic Characteristics of an Unsteady Separated Flow," AIAA Journal, **17**: 1332-1339.

Freymuth, P., Jackson, S. and Bank, W., [1988], "A Demonstration of Dynamic Stall Control," Flow Lines, TSI Incorporated, St. Paul, MN, Spring Issue.

Ghia, U., Zuo, L. and Ghia, K [1989], "Analysis & Control of Unsteady Separated Flows," Paper No. AIAA-89-1018, AIAA 2nd Shear Flow Conference, Tempe, AZ, March 13-16.

Helin, H.E. [1986], "Experimental Studies on Dynamic Development and Control of Unsteady Separated Flows," Ph.D. Thesis, University of Colorado.

Herbst, W.B. [1981], "Supermaneuverability," Joint Automatic Control Conference, Munich, Germany, June 17-19.

Huang, L.S., Maestrello, L. and Bryant, T.D. [1987], "Separation Control Over an Airfoil at High Angles of Attack by Sound Emanating From the Surface," Paper AIAA-87-1261, AIAA 19th Fluid Dynamics, Plasma Dynamics and Lasers Conference, Honolulu, HI, June 8-10.

Koga, D.J. [1983], "Control of Separated Flows Using Forced Unsteadiness," Ph.D. Thesis, Illinois Institute of Technology.

Koga, D.J., Nelson, C.F. and Eaton, J.K. [1987], "A New Program for Active Control of Unsteady, Separated Flow Structures," Proceedings of the AFOSR Unsteady Separated Flow Workshop II, Colorado Springs, CO, July 28-30.

Koochesfahani, M.M. and Dimotakis, P.E. [1988], "A Cancellation Experiment in a Forced Turbulent Shear Layer," Paper No. AIAA-88-3713, 1st National Fluid Dynamics Congress, Cincinatti, OH, July 25-28.

Liepmann, H.W. and Nosenchuck, D.M. [1982], "Active Control of Laminar-Turbulent Transition," J. Fluid Mech., **118**, pp. 201-204.

Luttges, M.W., Robinson, M.C. and Kennedy, D.A. [1985], "Control of Unsteady Separated Flow Structures on Airfoils," Paper AIAA-85-0531, AIAA Shear Flow Control Conference, Boulder, CO, March 12-14.

McCroskey, W.J. and Phillipe, J.J. [1975], "Unsteady Viscous Flow on Oscillating Airfoils," AIAA Journal, **13**: 71-79.

Nelson, C.F., Koga, D.J. and Eaton, J.K. [1987], "Phase-Averaged Measurements of the Unsteady, Separated Flow Behind an Oscillating Flap," presented at the 40th Anniversary Meeting of the Division of Fluid Dynamics, American Physical Society, Eugene, OR, November 22-24.

Nelson, C.F., Koga, D.J. and Eaton, J.K. [1989-a], "Unsteady, Separated Flow Behind an Oscillating Two-dimensional Flap," Paper No. AIAA-89-0288, AIAA 27th Aerospace Sciences Meeting, Reno, NV, January 9-12.

Nelson, C.F., Koga, D.J. and Eaton, J.K. [1989-b], "Control of the Unsteady, Separated Flow Behind an Oscillating, Two-Dimensional Flap," Paper No. AIAA-89-1027, AIAA 2nd Shear Flow Conference, Tempe, AZ, March 13-16.

Reisenthel, P.H. [1984], "Reattachment Control behind a Rearward- Facing Step Using Forced Unsteadiness," M.S. Thesis, Illinois Institute of Technology.

Reynolds, W.C. and Carr, L.W., [1985], "Review of Unsteady, Driven, Separated Flows," Paper AIAA-85-0527, AIAA Shear Flow Control Conference, Boulder, CO, March 12-14.

Ridgely, D.B. and Banda, S.S. [1986], "Introduction to Robust Multivariable Control," AFWAL-TR-85-3102 Final Report, Fluid Dynamics Laboratory, Wright-Patterson A.F.B., OH, February.

Shih, C., Lee, M. and Ho, C.M. [1987], "Unsteady Separation over Two and Three Dimensional Airfoils," Proceedings of the AFOSR Unsteady Separated Flow Workshop II, Colorado Springs, CO, July 28-30.

Spalart, P.R. [1988], "Vortex Methods for Separated Flows," NASA Tech. Mem. 100068, Ames Research Center, CA, June.

Spalart, P.R. and Leonard, A. [1981], "Computation of Separated Flows by a Vortex Tracing Algorithm," Paper No. AIAA-81-1246, AIAA 14th Fluid and Plasma Dynamics Conference, Palo Alto, CA June 23-25.

Viets, H., Piatt, M. and Ball, M. [1981], "Forced Vortices Near a Wall," AIAA 19th Aerospace Sciences Meeting, St. Louis, MO, January 12-15.

Walker, J.M. and Chou, D.C. [1987], "Forced Unsteady Vortex Flows Driven by Pitching Airfoils," Paper AIAA-87-1331, AIAA 19th Fluid Dynamics, Plasma Dynamics and Lasers Conference, Honolulu, HI, June 8-10.

Wygnanski, I.J. and Petersen, R.A., [1988], "Control of Free Shear Flows near Solid Surfaces", Research on Turbulence: AFOSR Contractors' Meeting, Los Angeles, CA, June 28-30.

Appendix A

FIGURES

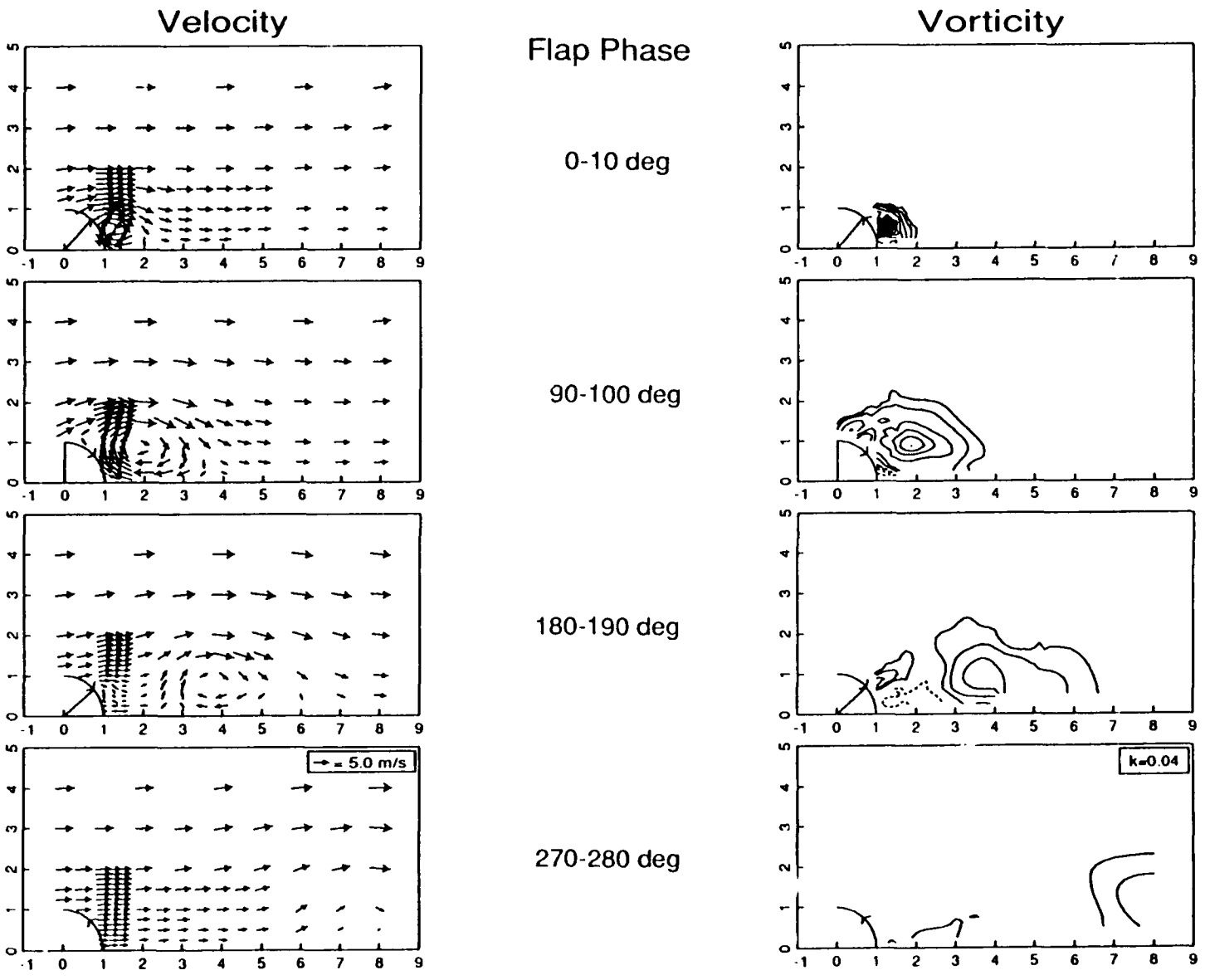

Figure 1. Velocity and Vorticity Field Maps for Oscillating Flap (k=0.04).

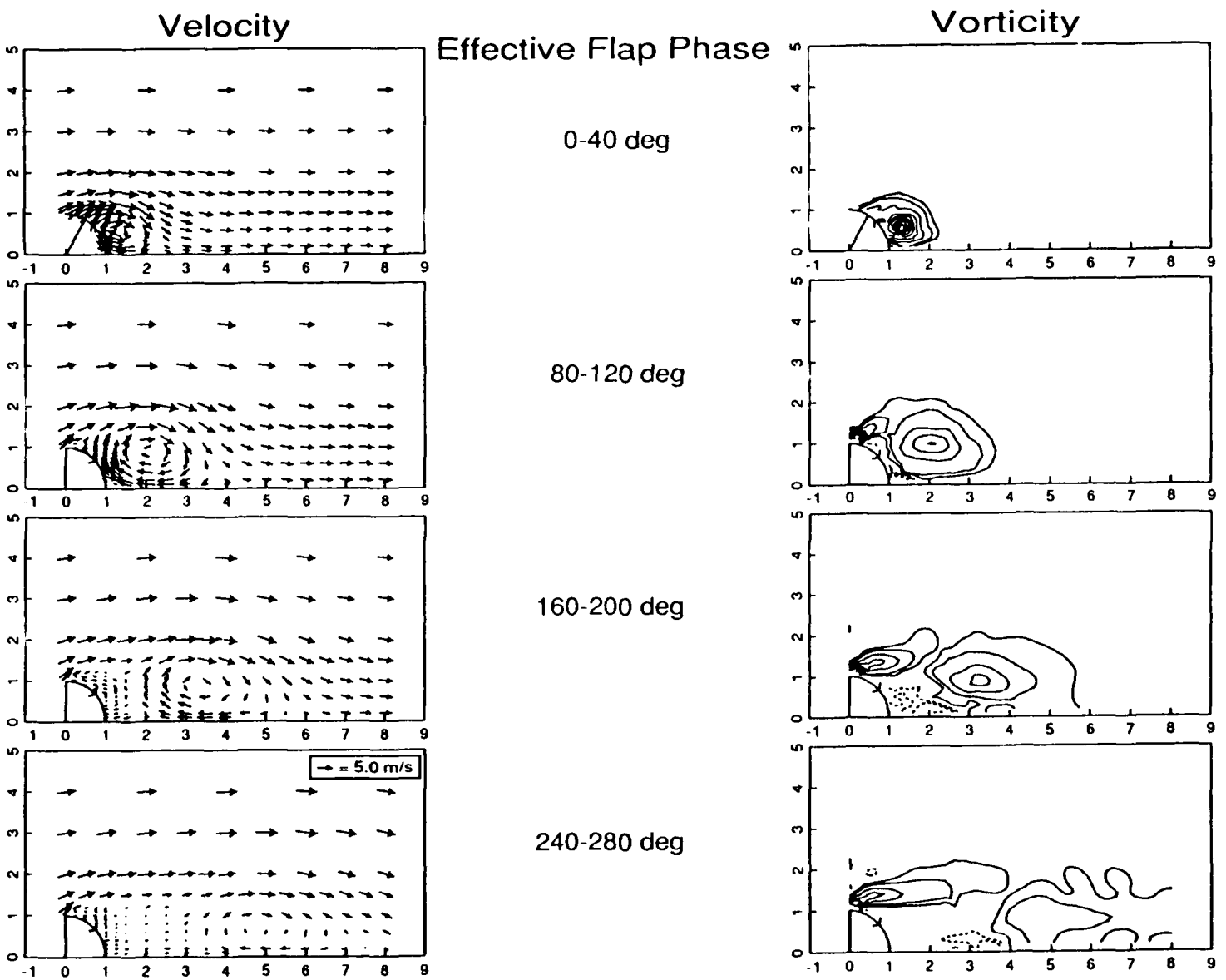

Figure 2. Velocity and Vorticity Field Maps for Pitch-and-Hold Flap (effective flap motion k'=0.04).

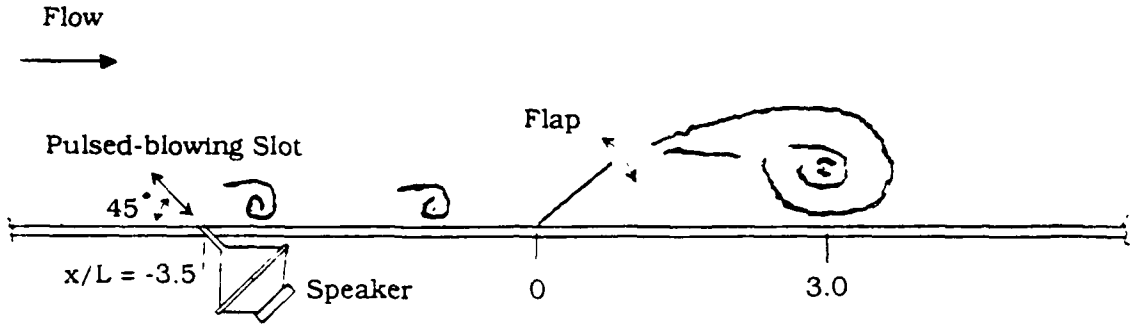

Figure 3. Schematic of Pulsed Blowing Control Experiment Apparatus.

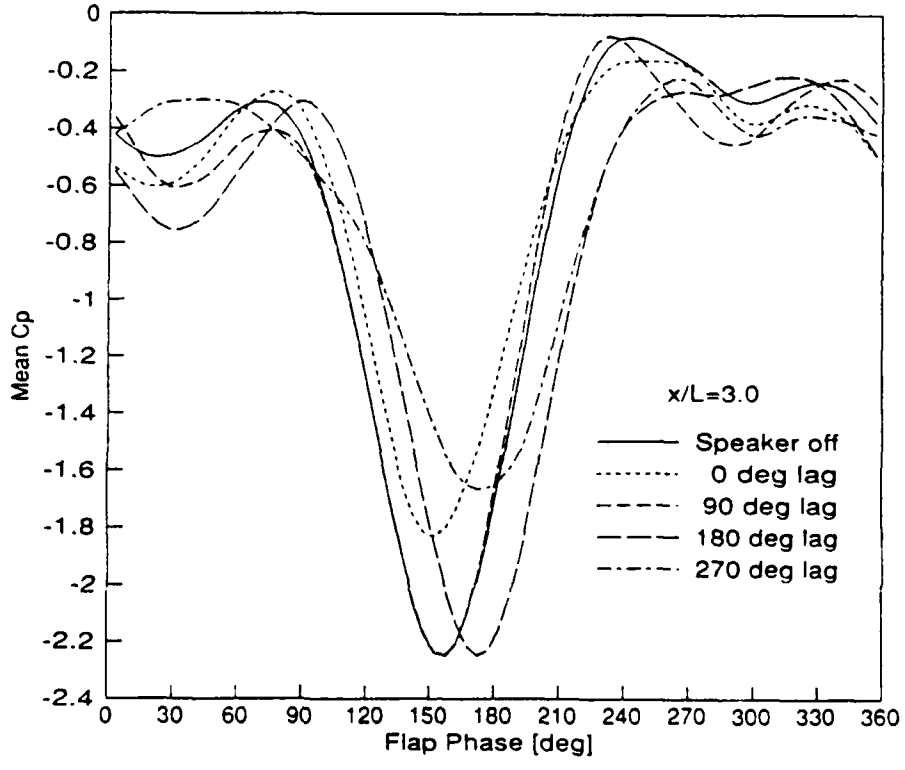

Figure 4. Phase-delay Vortex Control of Oscillating Flap Flow.

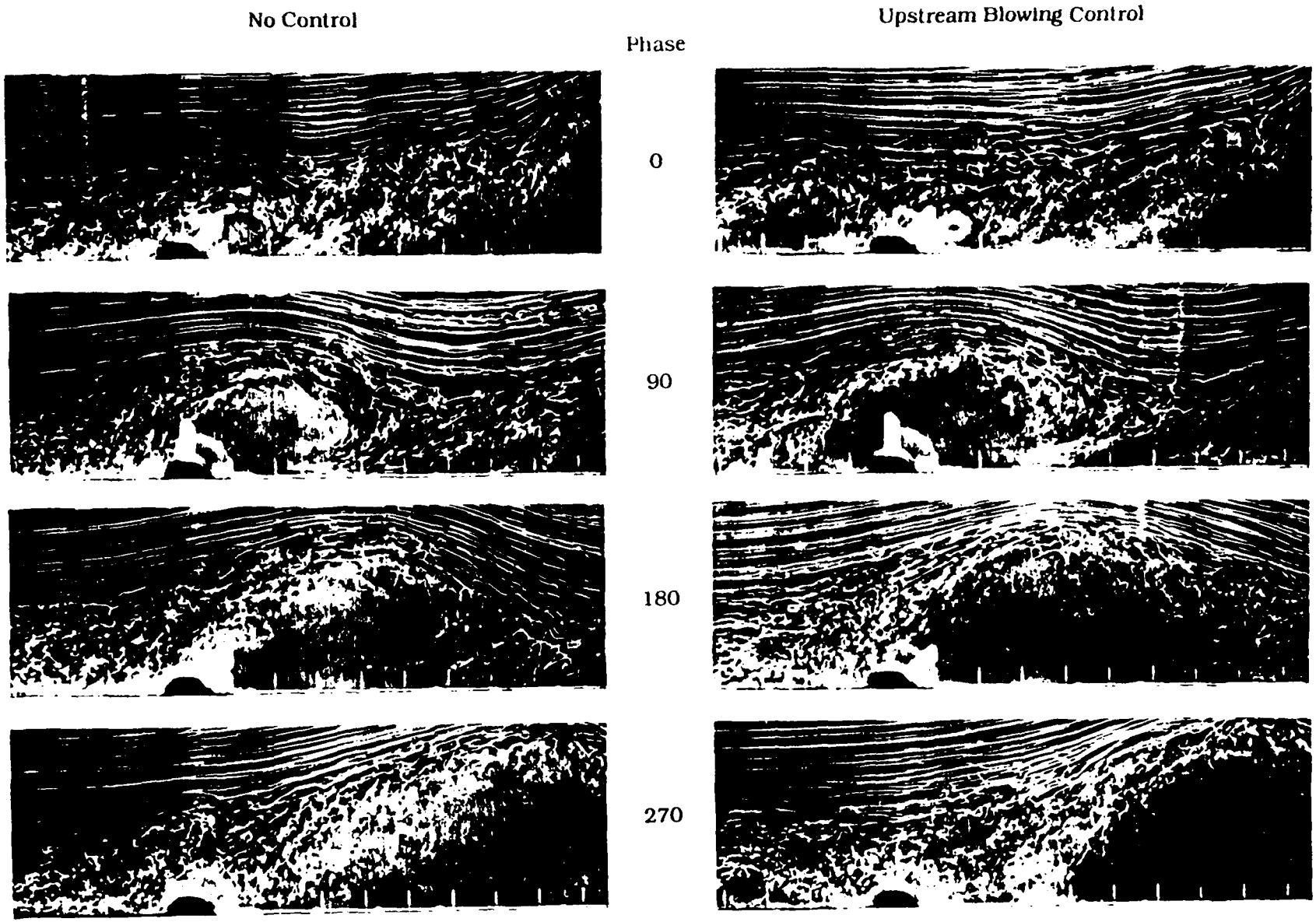

Figure 5. Smoke-wire Visualization of Pulsed-blowing Control Experiment.

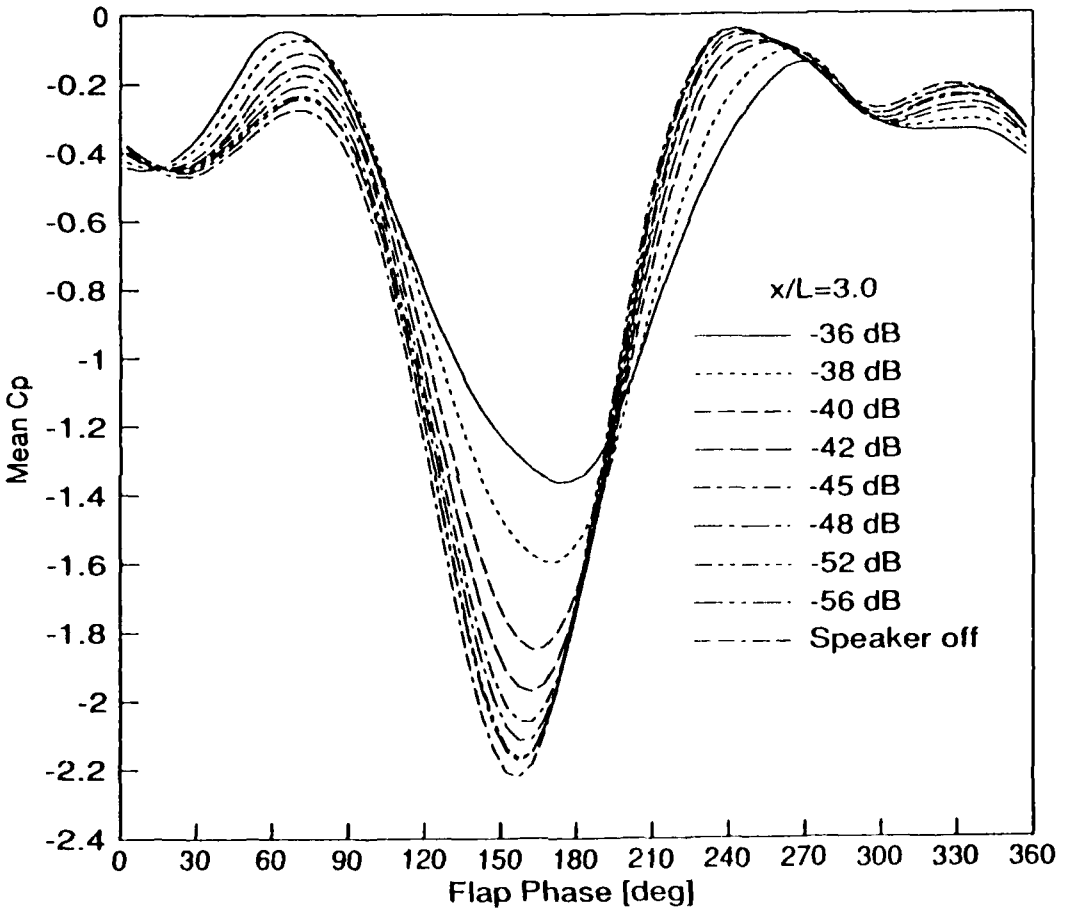

Figure 6. Proportional Control Effect of Pulsed-blowing Actuator.

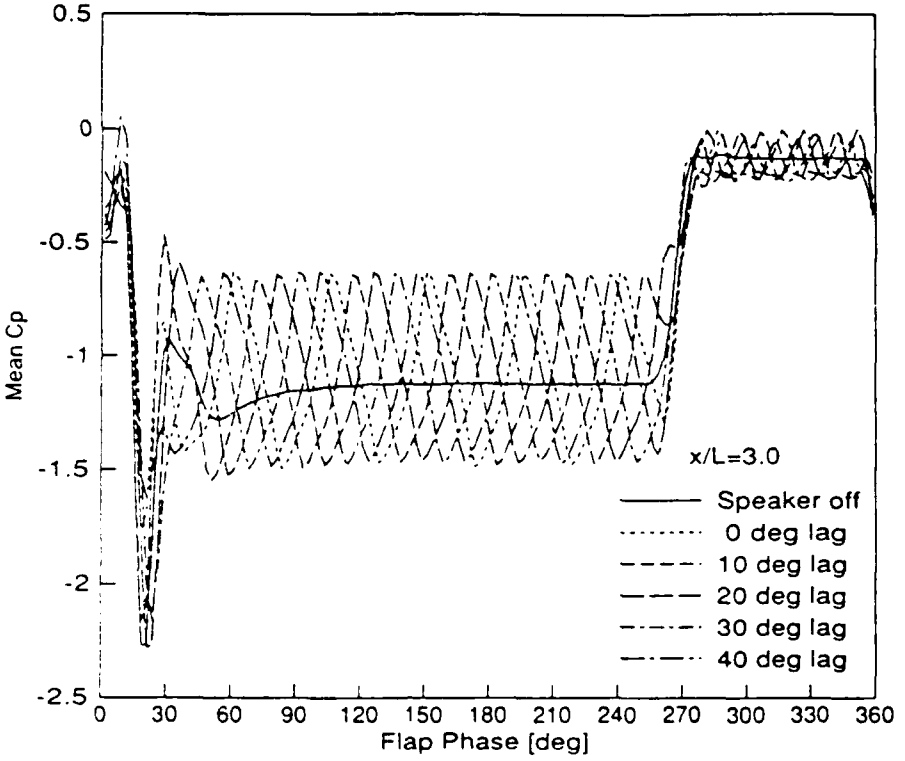

Figure 7. Phase-delay Control of Pitch-and-Hold Flap (full cycle).

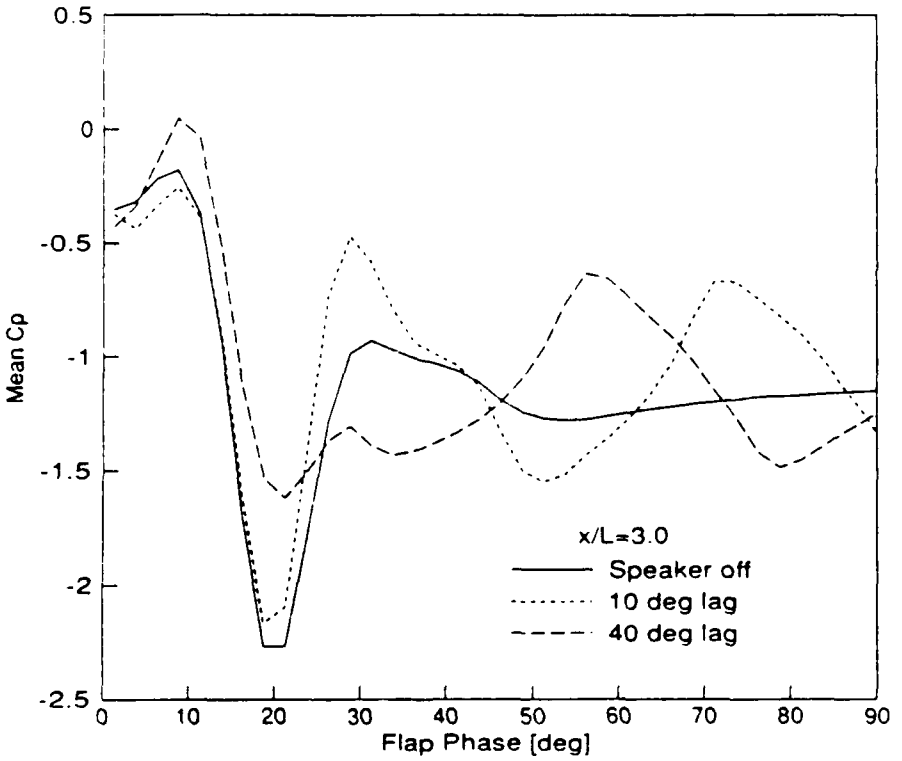

Figure 8. Phase-delay Control of Pitch-and-Hold Flap (expanded time).

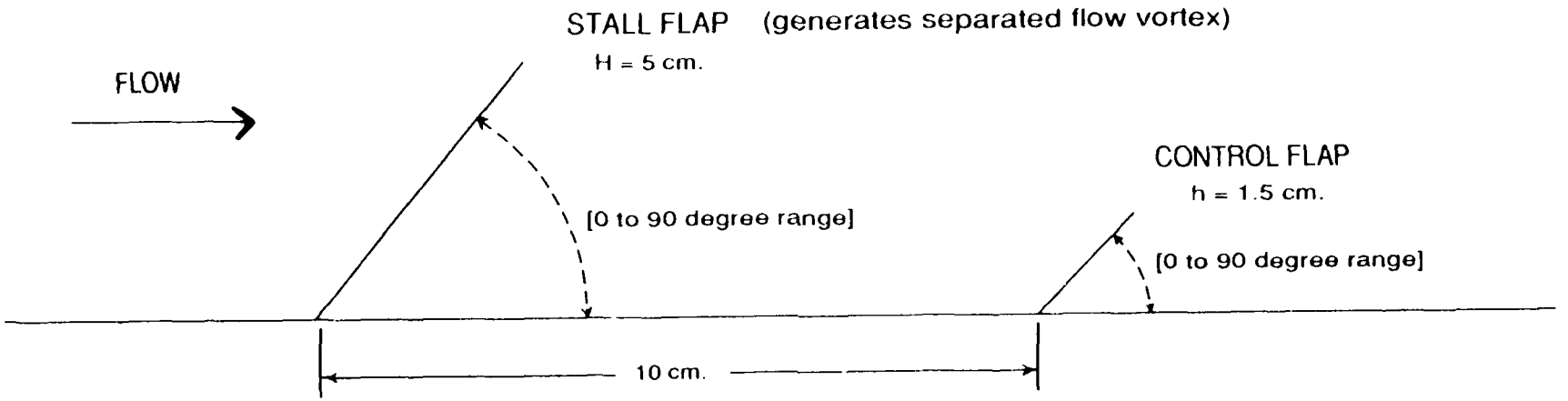

(a) Downstream Control Configuration

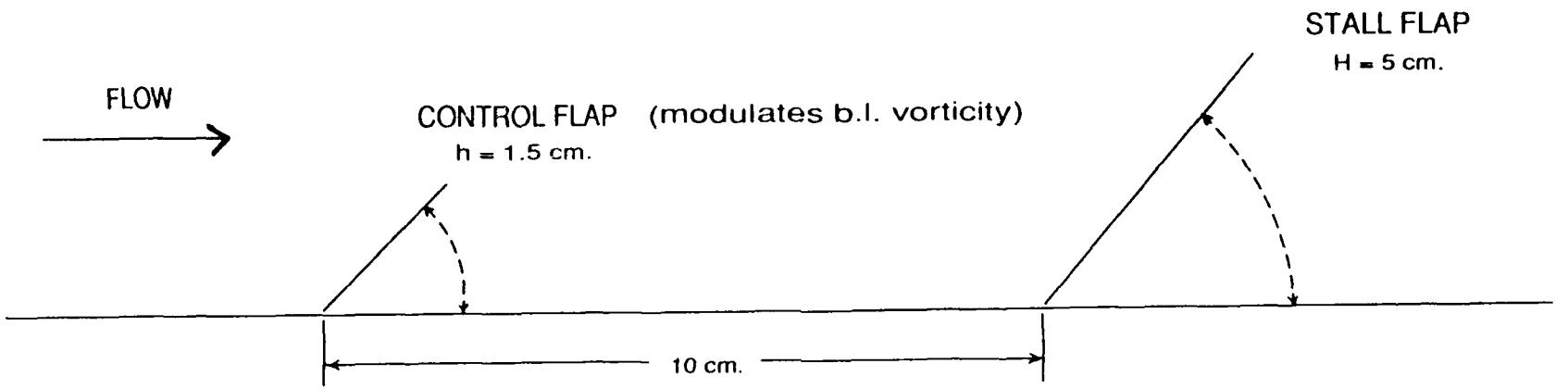

(b) Upstream Control Configuration

Figure 9. Schematic of Dual-Flap Configurations.

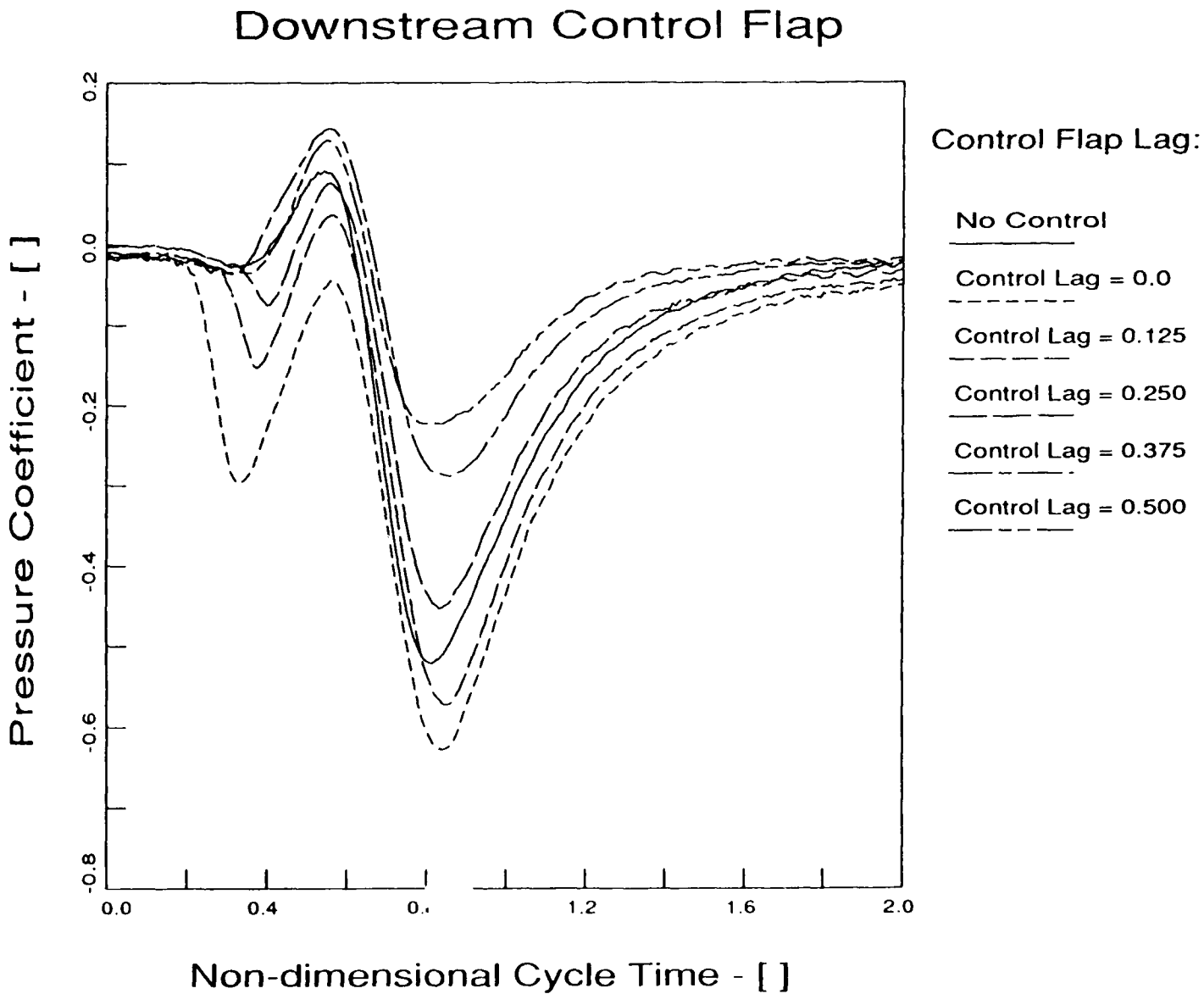

Figure 10. Vortex Pressure Signatures with Downstream Control Flap.

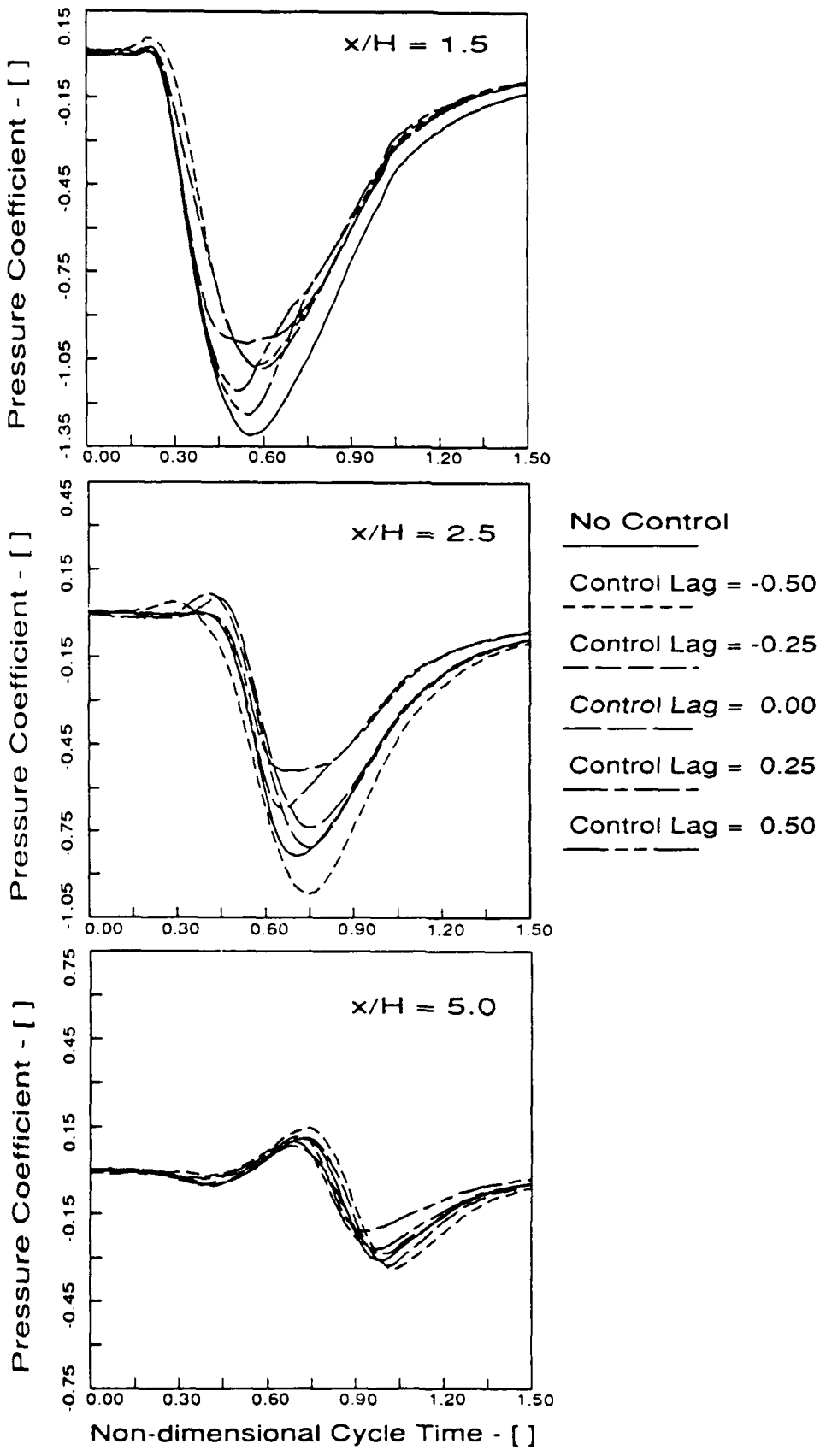

Figure 11. Control Effect Propogation as Vortex Convects Downstream.

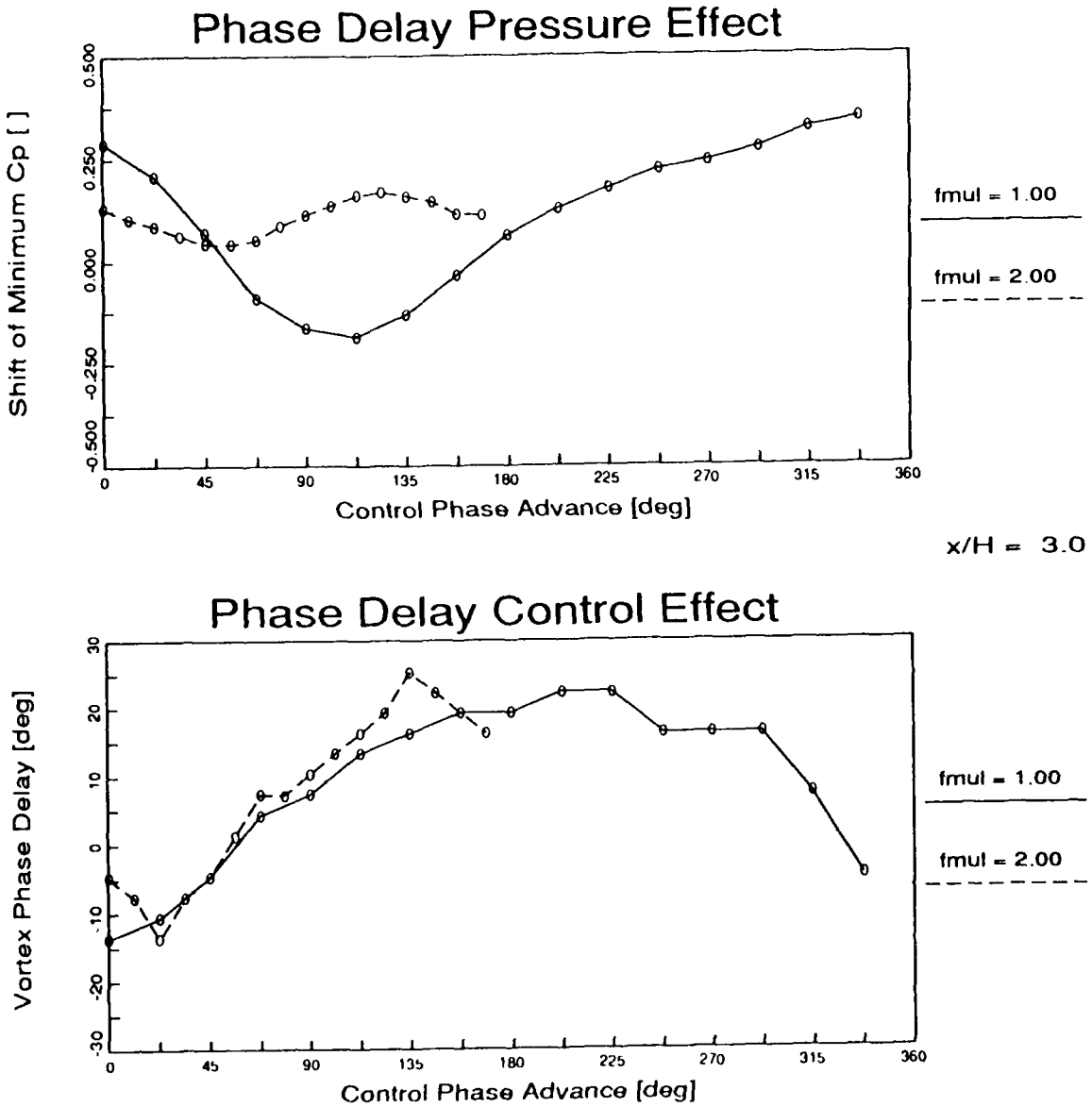

Figure 12. Vortex Control Effects for Continuous Sinusoidal Flap Motions.

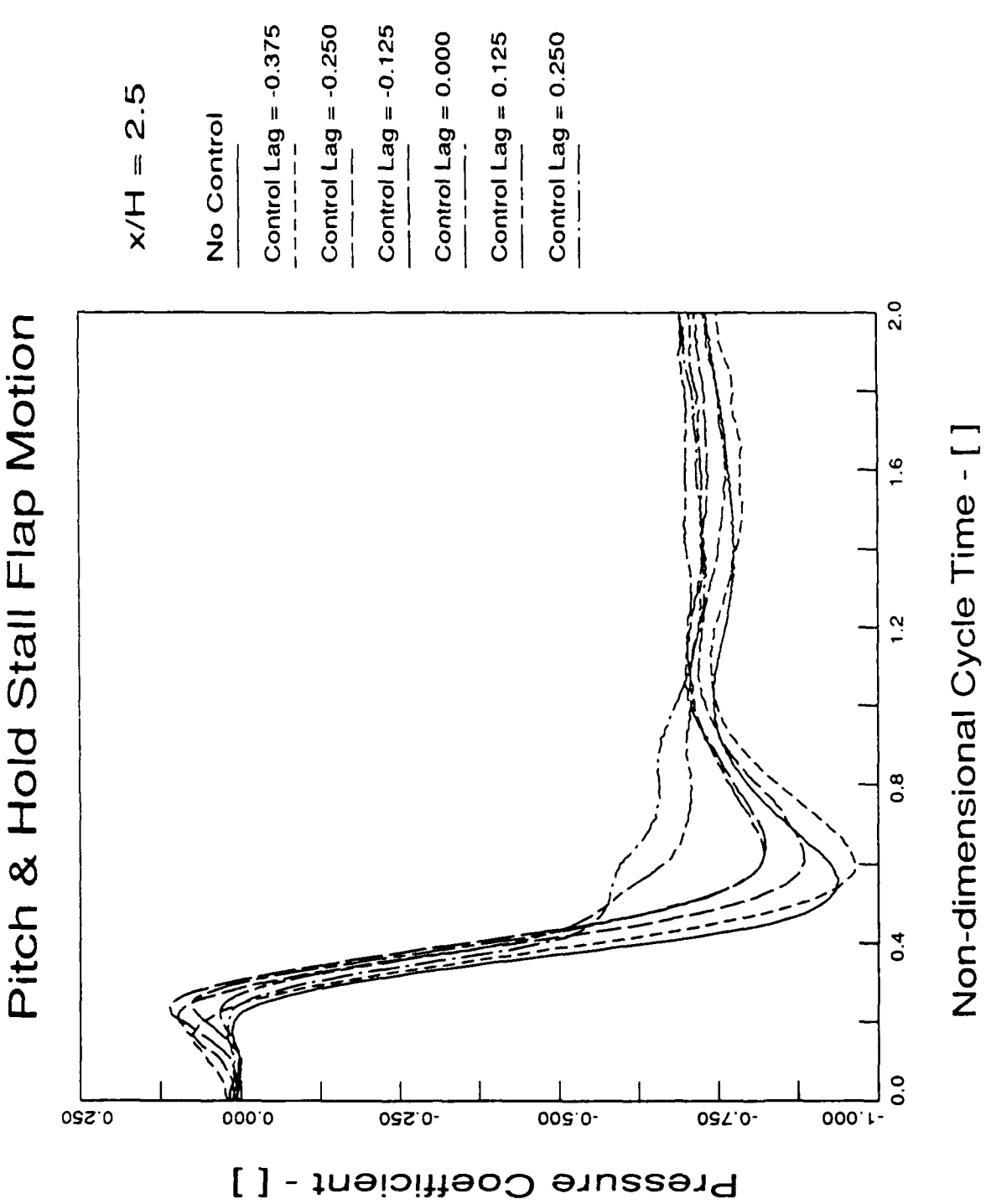

Figure 13. Control Flap Effect on Pitch and Hold Stall Flap Motion.

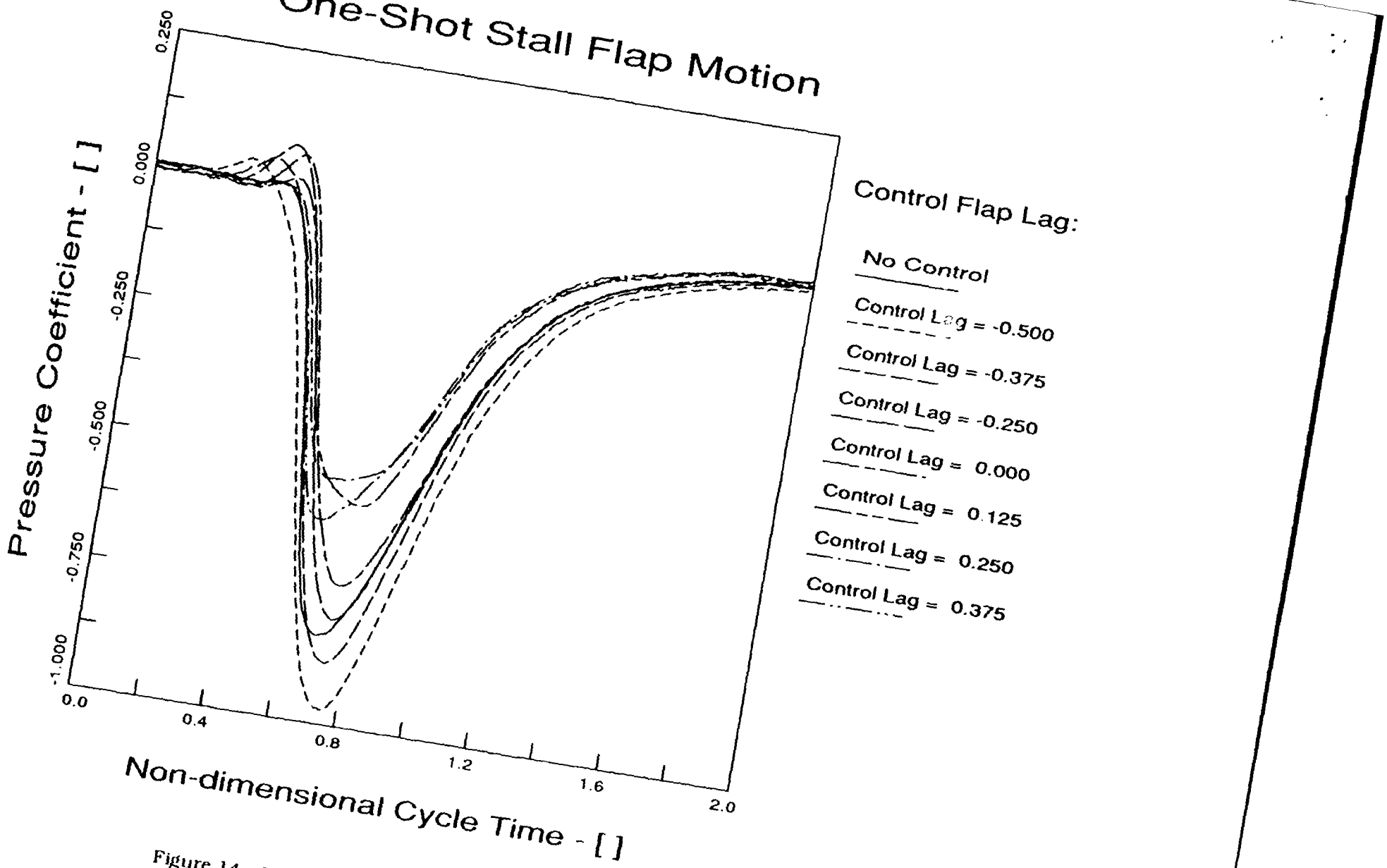

Figure 14. Control Flap Effect on One-shot Stall Flap Motion.

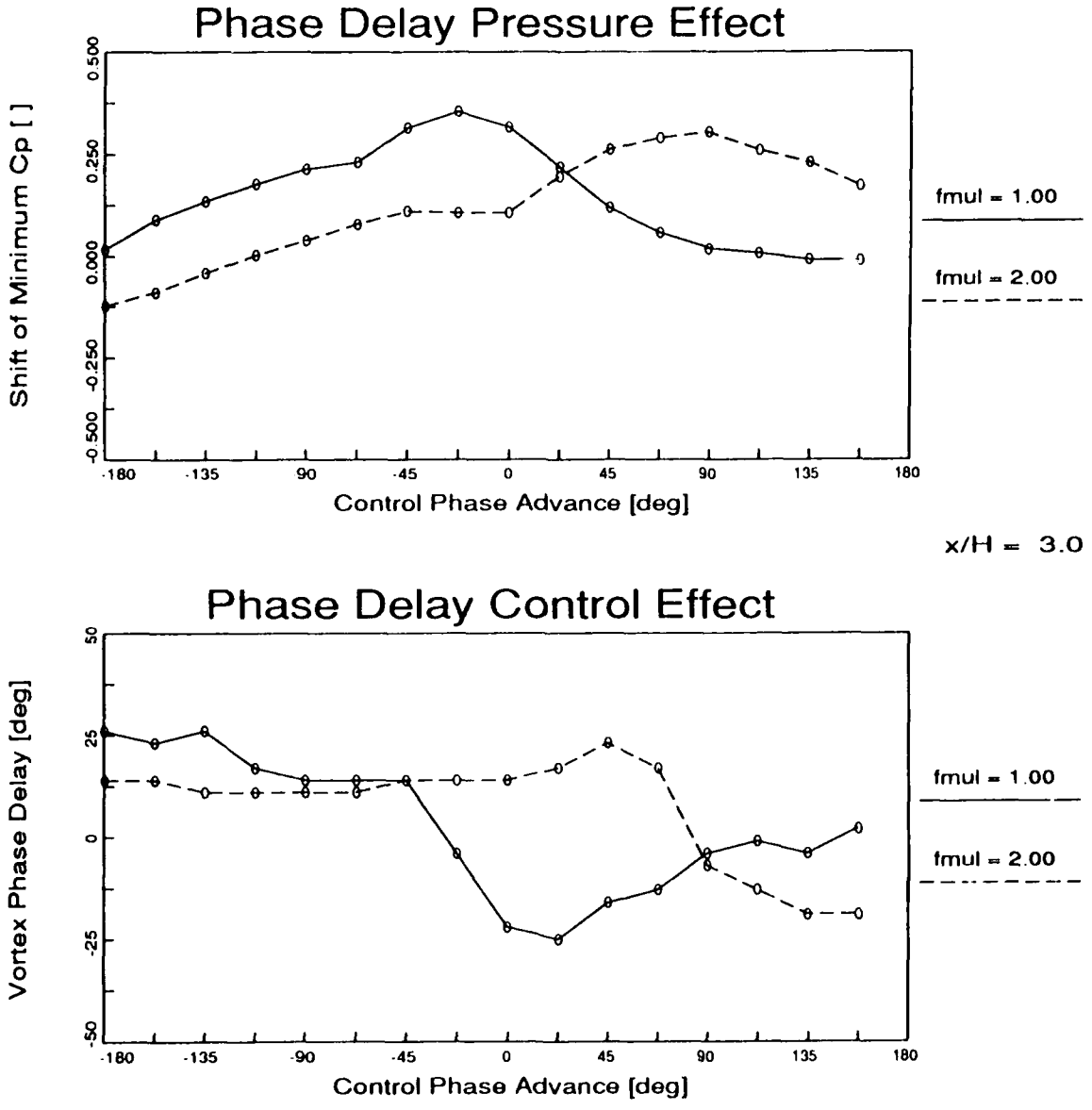

Figure 15. Vortex Control Effect for One-shot Flap Motions.

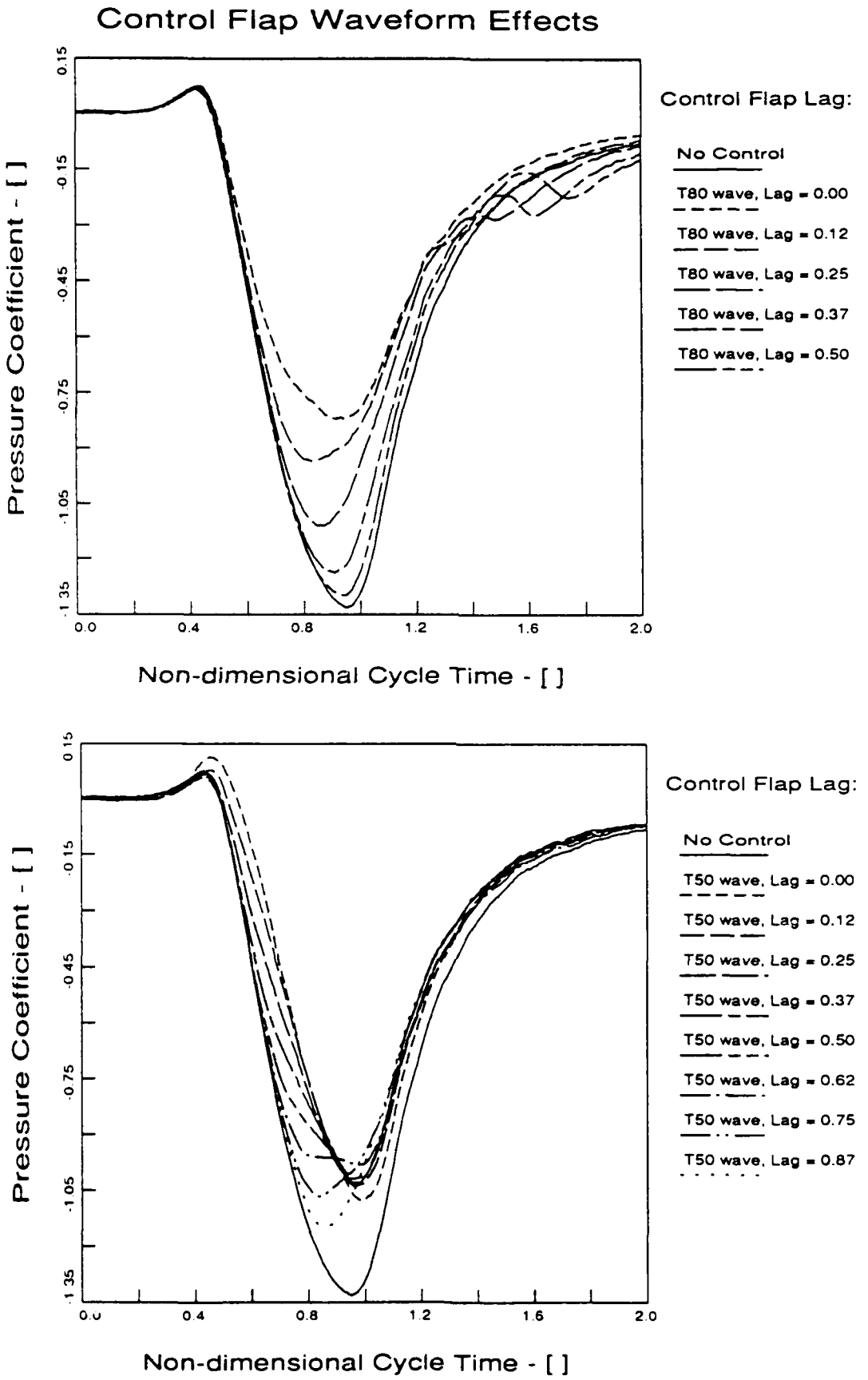

Figure 16. Effect of Control Flap One-shot Waveform Shape.

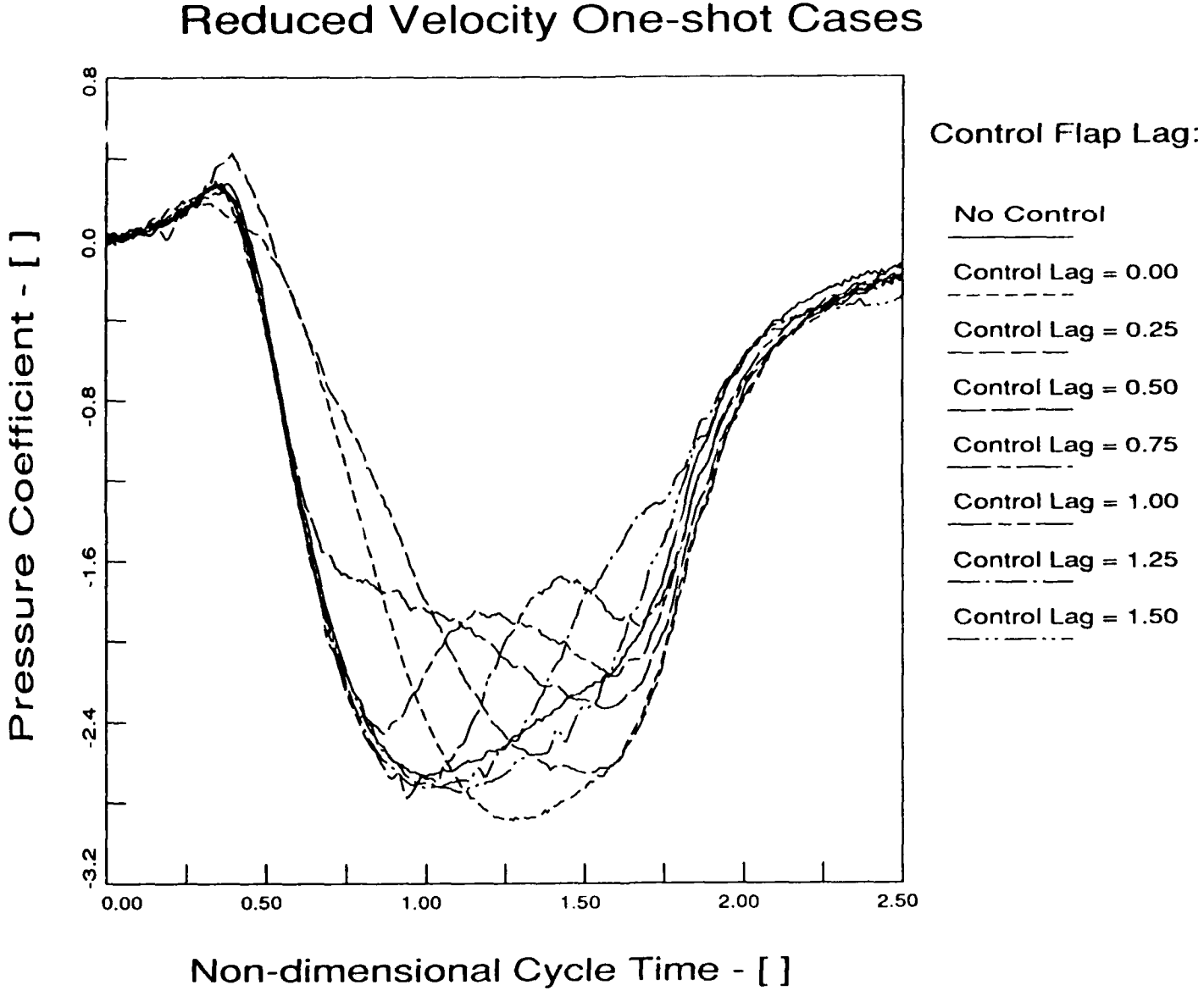

Figure 17. Vortex Control Effectiveness at Reduced Freestream Velocity.

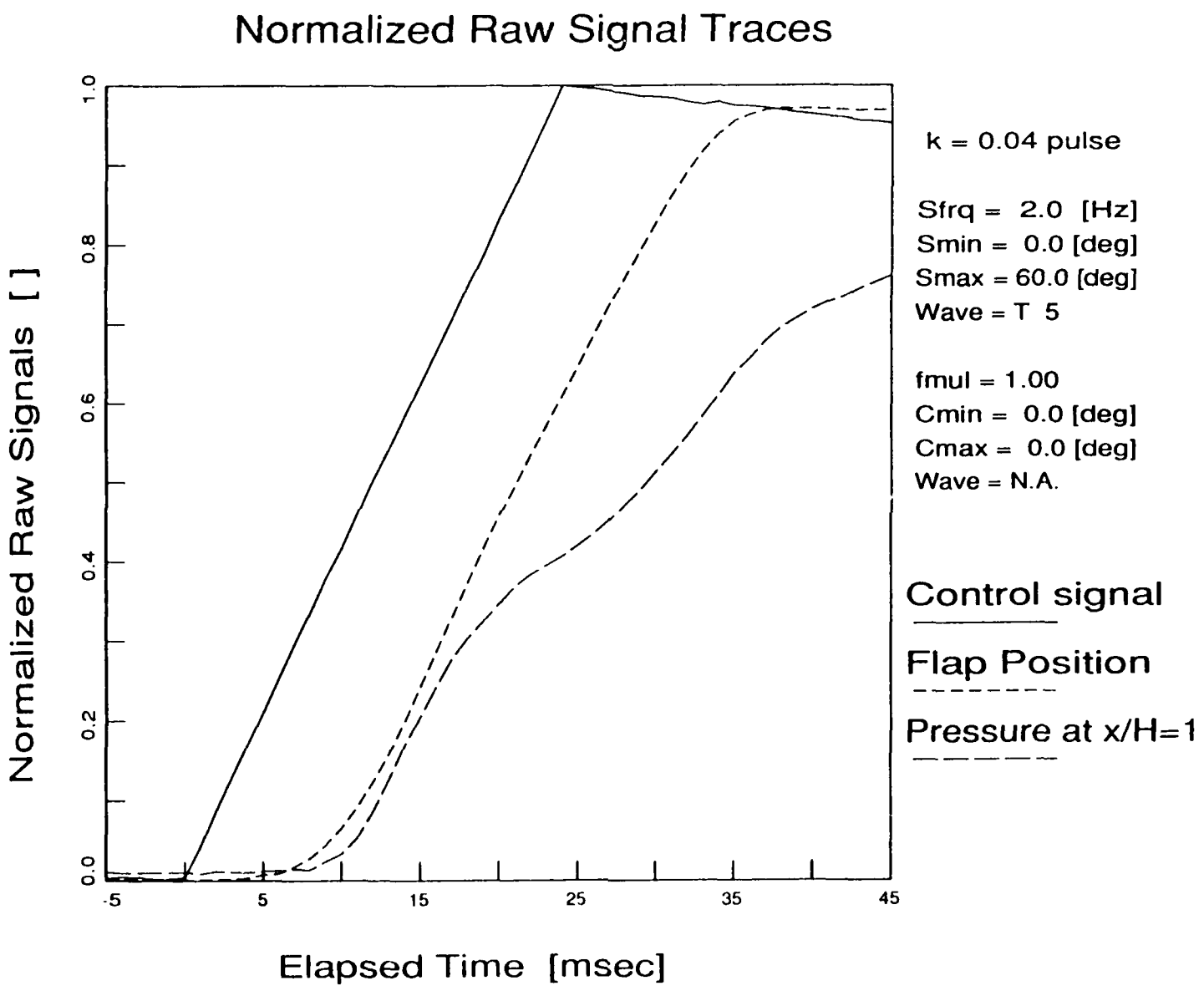

Figure 18. Time-lag Response of Flap Actuator and Pressure Sensor.

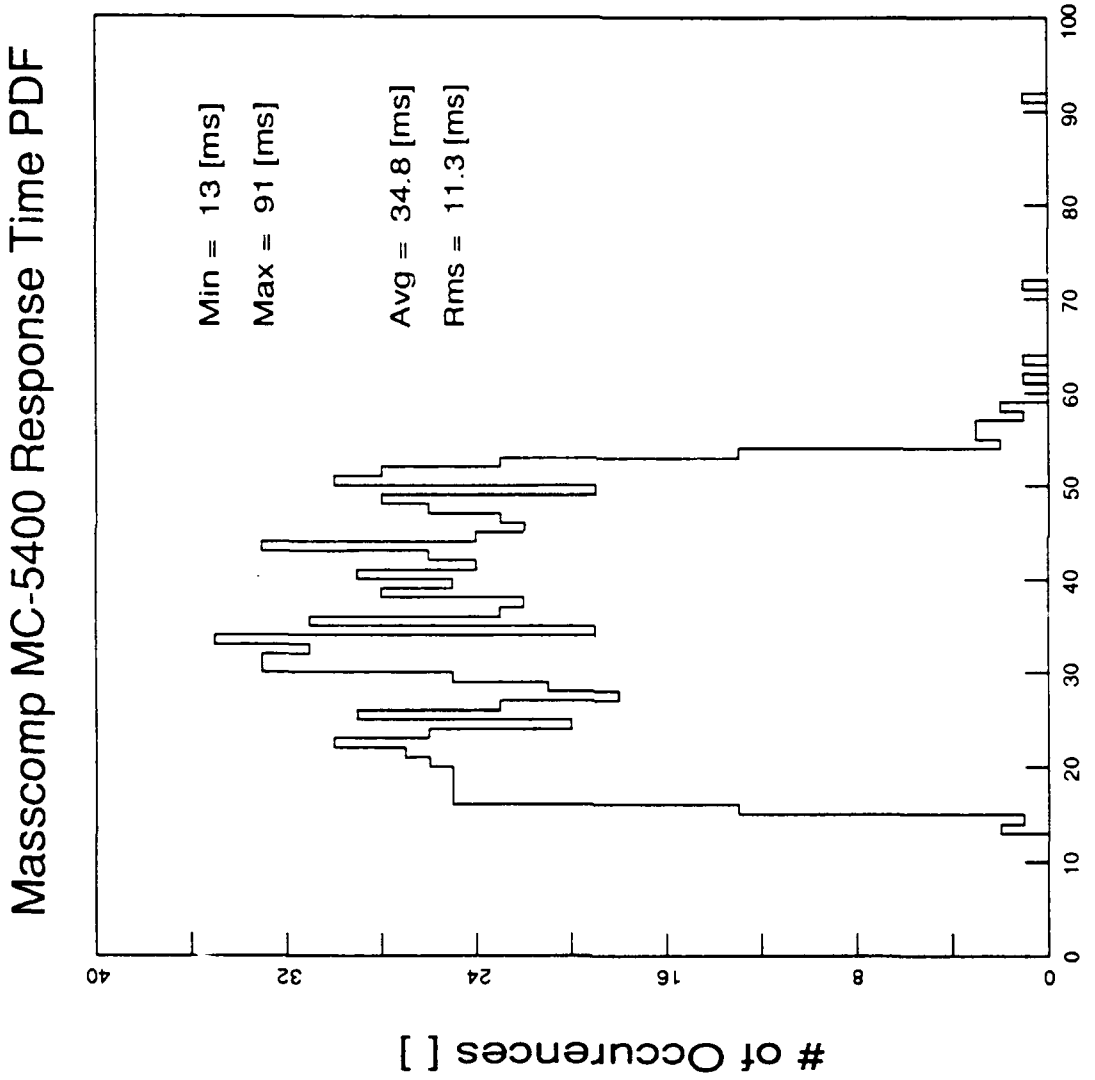

Figure 19. Interrupt Response PDF for Masscomp MC-5400 UNIX-based system.

Appendix B

COPIES OF SELECTED RESEARCH PROGRAM PUBLICATIONS

AIAA '89

AIAA 89-0288
Unsteady, Separated Flow Behind An Oscillating Two-Dimensional Flap

C. Nelson, D. Koga and J. Eaton,
Stanford Univ., Stanford, CA

27th Aerospace Sciences Meeting
January 9-12, 1989/Reno, Nevada

AIAA-89-0288

UNSTEADY, SEPARATED FLOW BEHIND AN OSCILLATING, TWO-DIMENSIONAL FLAP

Curtis F. Nelson*, Dennis J. Koga+ and John K. Eaton++

Department of Mechanical Engineering
Stanford University
Stanford, CA 94305-3030

ABSTRACT

Unsteady, separated flow produced behind a two-dimensional, lifting flap was examined in detail using phase-averaged LDA and surface pressure measurements. Both sinusoidal oscillations with reduced frequencies in the range 0.025 to 0.06 and pitch-and-hold motions of the flap were investigated. Phase-averaged vorticity was calculated from the velocity data and the development of the unsteady vortex formed downstream of the flap was analyzed. The dominant mechanism of vorticity transport is shown to be convective, justifying the use of discrete-vortex computations for modeling this flow.

NOMENCLATURE

c_p	Pressure coefficient, $(P-P_{ref})/(\rho U_{ref}^2/2)$
f	Frequency of the flap oscillation cycle [Hz]
k	Reduced frequency based on flap length, $k=fL/U_{ref}$
L	Flap chord length = 25.4 mm
P	Static pressure on the bottom wall of the tunnel
P_{ref}	Reference (free-stream) static pressure
t	Time (t=0 when the flap is flush with the tunnel bottom and just starting to rise)
U_{ref}	Reference velocity (tunnel centerline velocity)
u	Velocity component in the x-direction
v	Velocity component in the y-direction
x	Streamwise distance downstream of the flap rotation axis
y	Vertical distance from the bottom wall of the tunnel
z	Spanwise distance from the tunnel centerline
θ	Flap rotation angle
φ	Phase in the oscillatory flap cycle, where $\varphi=0$ is always at the point $\theta = (\theta_{min}+\theta_{max})/2$ when the flap is rising from the wall
ω_3	Spanwise vorticity = $\partial v/\partial x - \partial u/\partial y$
Γ	Circulation
$\overline{(\ )}$	Phase-averaged component; it is the average of a quantity when taken at the same point, or phase, in each cycle of a record of many cycles
$(\ )'$	Turbulent component

1. INTRODUCTION

The flow behind a two-dimensional, lifting flap serves as a simple model of more general unsteady, separated flows and also has practical application in its own right. It has been recognized that large vortical structures are the dominant feature in these flows and that the unsteady effects produced by these structures can be either beneficial or detrimental to overall device performance. For example, the initial flow structure which rolls up behind the flap creates a strong spanwise vortex, a corresponding negative pressure on the surface, and a substantial short term lift augmentation. If the flap remains up long enough, a steady separation is formed as the vortex either sheds or decays, and the lift augmentation is lost. Coherent structures in the separated shear layer, though not strong enough to cause lift augmentation, can cause substantial buffeting. Understanding and manipulation of the unsteady flow structures would enable one to take advantage of the beneficial effects while mitigating the detrimental effects.

Previous researchers have investigated related unsteady flows generated by moving control surfaces, usually in an attempt to dynamically reattach an otherwise separated flow. These studies have typically used flow visualization, surface pressures, and hot-wire anemometry as the means of acquiring the data. Francis, *et al.*[1] studied the unsteady flowfield generated by the oscillation of a fence-type spoiler on an airfoil using a hot-wire anemometer. Consigny, *et al.*[2] studied the effects of different motions of a hinged spoiler on the pressure distribution on a supercritical airfoil, this work was later extended by adding an unsteady, trailing-edge flap[3]. Viets, *et al.*[4] used flow visualization and hot-wire measurements to study the flowfield generated by a rotor mounted on a wall. Huyer, *et al.*[5] used flow visualization and hot-wire anemometry to study an airfoil with a periodically deformable leading edge in order to promote reattachment past the static stall angle of attack.

Previous work on the lifting flap flow by Koga[6] and Reisenthel, *et al.*[7] used smoke-wire flow visualization combined with surface pressure and hot-wire measurements to identify the frequency range for the production of large coherent vortices. They also studied using vortices produced by the lifting flap in order to reduce the reattachment length of a steady separation for various configurations. Ahmed, *et al.*[8] investigated the time development of the separated region for a rapidly-rising, lifting flap using surface pressure measurements. Computational studies have used inviscid flow models, such as the discrete-vortex method, to calculate flows behind lifting and oscillating flaps[9,10]. Such inviscid methods work well if the flap descends before the large vortex begins to diffuse substantially.

The objectives of the present study were to obtain detailed velocity measurements using a laser-Doppler anemometer (LDA) in the unsteady and separated flow region behind an oscillating flap. Special emphasis was placed on the unsteady reversing flow just behind the flap since reliable hot-wire measurements are not possible in this region. Both sinusoidal flap waveforms and a waveform in which the flap pitches up rapidly then holds in the extended position have been examined. The velocity measurements will be used for understanding the basic mechanisms operative in unsteady, separated flows and for comparison to computational methods.

2. EXPERIMENTAL TECHNIQUES

The experiments were performed in a low-speed, 150 mm x 450 mm, open-circuit wind tunnel used in earlier backward-facing step flow experiments[11]. The test section was modified to eliminate the step and install the flush

---

* Research Assistant, Student Member AIAA
\+ Senior Research Associate, Member AIAA
++ Associate Professor and Associate Chairman, Member AIAA

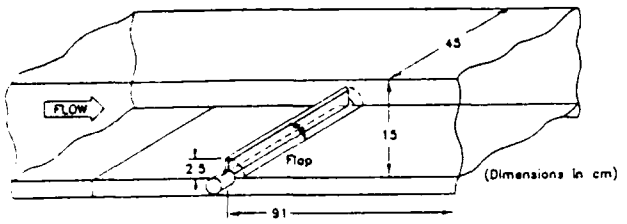

FIGURE 1. Schematic of Wind Tunnel Geometry

mounted flap. The approach flow was tripped on all four tunnel walls and the boundary layers are allowed to develop over a 3.5 m length. The side wall boundary layers were removed approximately 27 flap lengths upstream of the flap to maintain a two-dimensional approach flow. At the nominal free-stream velocity of 5 m/s, the Reynolds number based on flap chord is 8200, and the boundary layer momentum thickness Reynolds number is 1900.

The two-dimensional flap is located on the bottom wall of the tunnel and spans the test section as shown in Figure 1. The flap aspect ratio (span/chord) was 18 to ensure two-dimensionality of the separated region[12]. The flap was actuated by a computer-controlled servo system driving a printed-circuit motor directly connected to the flap shaft and was free to oscillate from a position flush with the bottom surface of the tunnel (θ=0°) to a position perpendicular to the bottom wall (θ=90°). The flap waveform was specified by loading appropriate position information into computer memory and sending the signal out through a digital-to-analog converter. Flap position and velocity feedback were provided by an RVDT and a tachometer both mounted directly to the flap shaft.

The flowfield in the periodically separated region downstream of the oscillating flap was examined using smoke-wire flow visualization, surface pressure measurements, and laser anemometry. Flow visualization showed that the flow structure was very repeatable from cycle to cycle, thus all measurements were phase-conditioned on the phase of the flap motion. Pressure measurements were made using a Validyne CD15 carrier/demodulator and a Validyne DP-45 pressure transducer connected differentially between the tunnel floor and the free-stream static pressure. The LDA measurements were made using a single component, Bragg-shifted, forward scattering system[13]. The beams were rotated to acquire either the u- or v-component of the velocity. A TSI Model 1980 counter processor was used to measure the Doppler frequency and the LDA data was acquired using a 16-bit parallel digital data port. Condensed mineral oil vapor droplets were supplied upstream of the wind tunnel blower for LDA seeding.

Special handling of the velocity data was required since the seed particles arrive at the LDA measurement volume at random phases of the flap cycle. Flap phase information was acquired simultaneously with each velocity sample. The data was then placed into phase bins and the velocity averaged over all the samples in a given bin. Typically 50,000 samples were acquired at each measurement point for each velocity component and phase-averaged into 36 bins. This usually required the acquisition of data over a minimum of 300 flap cycles for the sinusoidal flap motions and 100 cycles for the pitch-and-hold motion. A field of data consists of two-components of velocity at each of 74 to 160 measurement points.

The phase-averaged vorticity was calculated by fitting the two-dimensional velocity field for each phase bin with natural cubic splines in both directions and analytically differentiating the splines. Data acquisition and processing were done on a Masscomp MC-5500 computer system.

3. RESULTS AND DISCUSSION

The data consist of phase-averaged velocity and vorticity fields along the centerline plane of the wind tunnel and the corresponding phase-averaged surface pressures on the bottom wall of the tunnel for four different cases, all at a nominal free-stream velocity of 5 m/s:

(1) 5 Hz sinusoidal oscillation (k=0.025) from θ=0° to 90°.
(2) 8 Hz sinusoidal oscillation (k=0.04) from θ=0° to 90°.
(3) 12 Hz sinusoidal oscillation (k=0.06) from θ=10° to 80°.
(4) Pitch-and-hold motion (effective k=0.04) from θ=0° to 90°.

Figure 2 shows the relationship between flap angle and flap phase for the two types of flap waveforms investigated (note that a phase difference of 360° for a 5 Hz waveform corresponds to a 0.2 second time difference compared to 0.125 seconds for an 8 Hz waveform). These reduced frequencies are rather low as the maximum speed of the flap tip is only 23% of the free-stream speed for the highest reduced frequency investigated. The pitch-and-hold motion is actually a 1 Hz cycle (360° flap phase = 1 sec) that starts as though it were an 8 Hz sinusoid (effective k=0.04) except the flap holds for 0.675 seconds once it reaches its maximum extension. After the flap returns to the wall as an 8 Hz sinusoid, it remains flush with the bottom wall of the tunnel for 0.2 seconds in order for the flow to re-establish itself before the start of the next cycle.

3.1. Unsteady Velocity and Vorticity

The results of these four cases have been condensed into a series of computer-animated movies which show the time evolution of the unsteady vortex during the flap cycle. Frames from these animations in Figures 3 through 6 clearly show that the flow is dominated by the presence of a large, unsteady vortex. Note that velocity vectors are plotted only at points where data was taken.

As the flap rises away from the wall a strong vortex is formed and negative velocities with magnitudes larger than the free-stream velocity are observed. The vortex grows until the flap reaches its maximum extension away from the wall. When the flap begins to move back towards the wall, the vortex is released and convects downstream. As the vortex convects, its peak vorticity decays rapidly due to viscous or turbulent diffusion. As shown in Figures 3 through 5, the size of the vortical region formed behind the flap increases as the reduced frequency of the flap rotation is decreased. This follows from the fact that there is more time for boundary layer vorticity to accumulate in the separated vortex as the flap frequency is reduced. At the low reduced frequencies, the

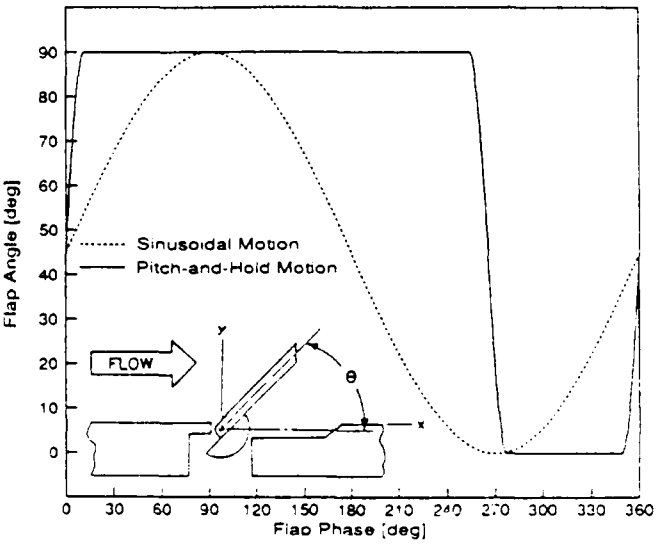

FIGURE 2. Flap Waveforms

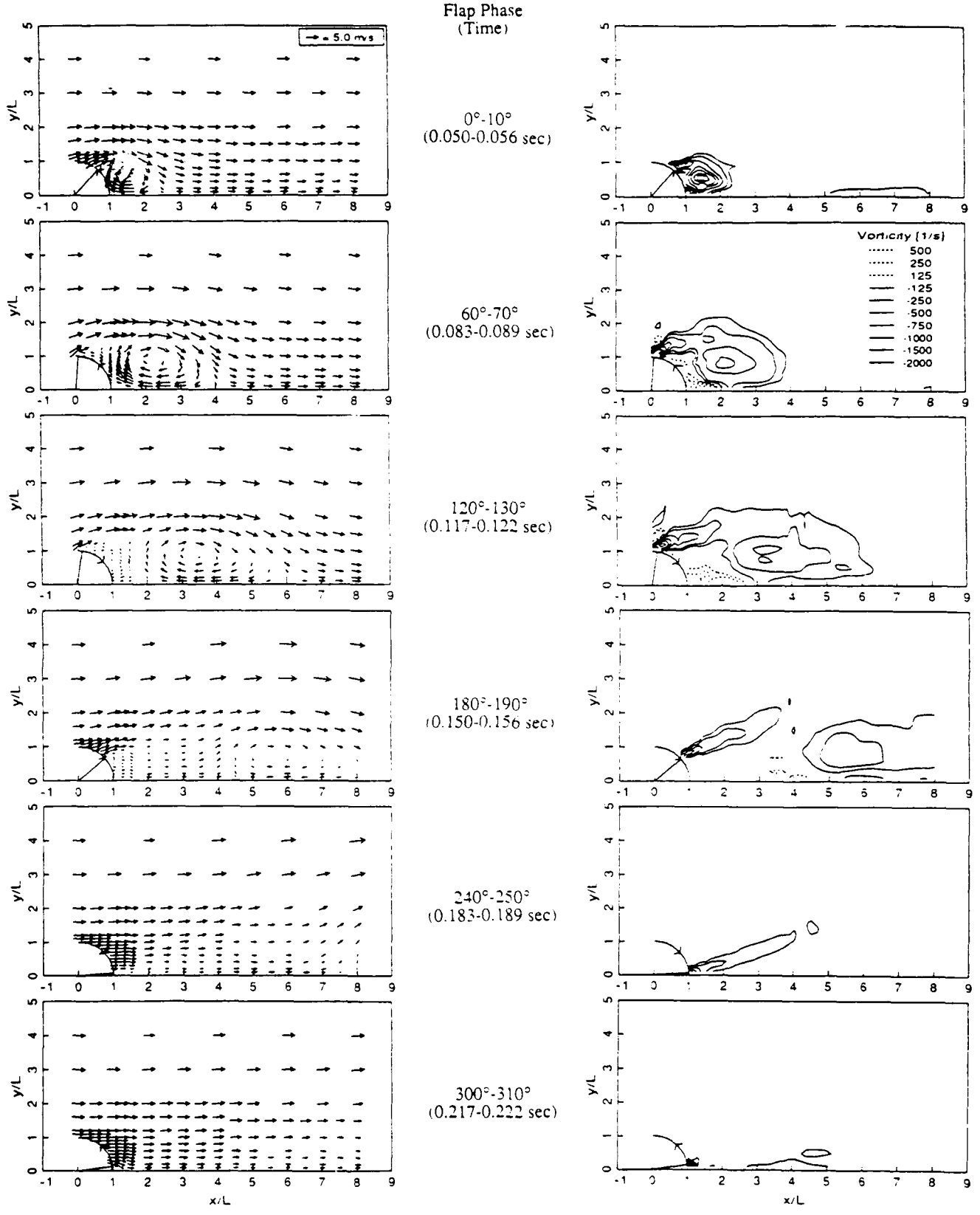

(a) Velocity Data

(b) Calculated Vorticity

FIGURE 3. Unsteady Flowfield for 5 Hz Sinusoidal Flap Motion (k=0.025)

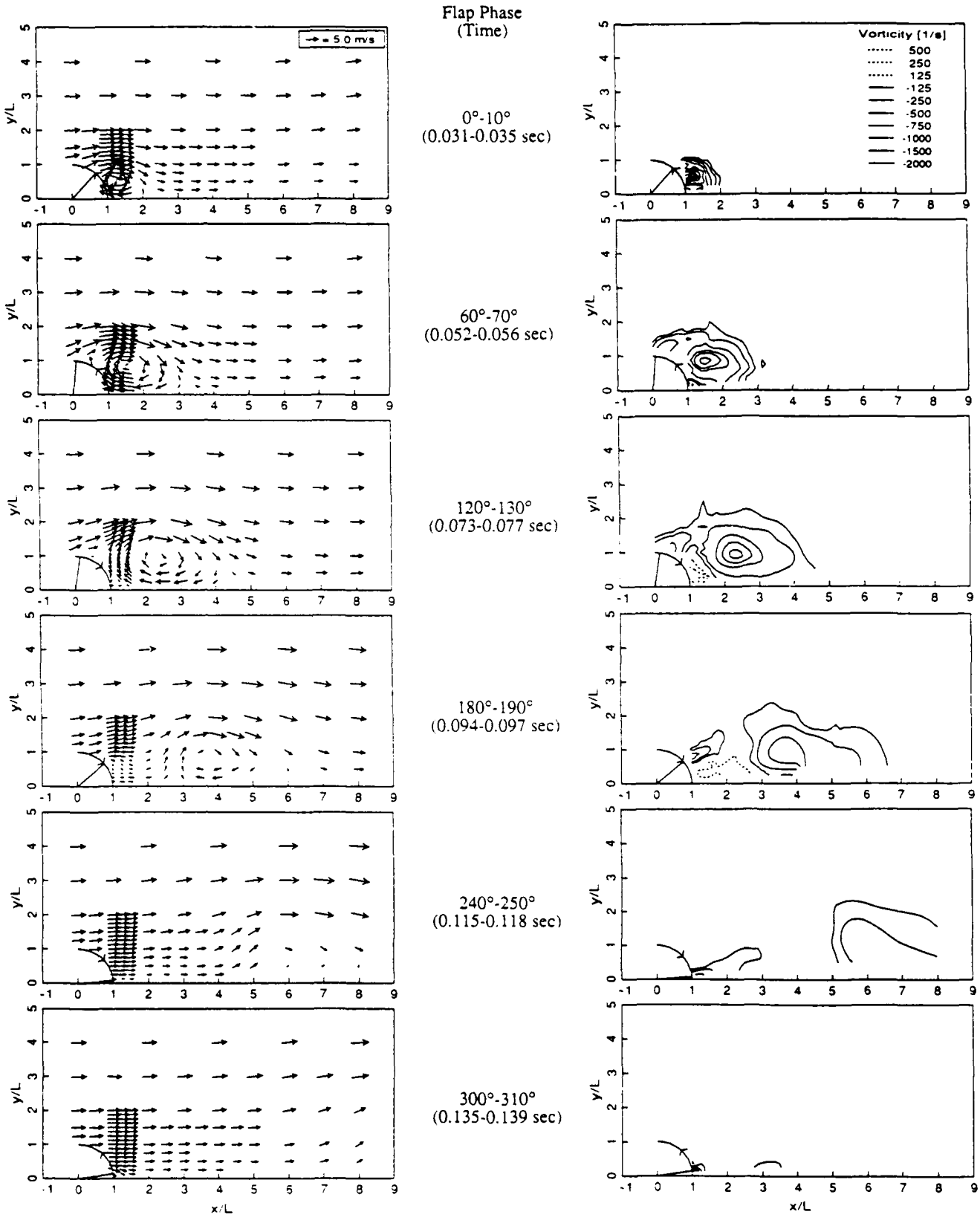

(a) Velocity Data

(b) Calculated Vorticity

FIGURE 4. Unsteady Flowfield for 8 Hz Sinusoidal Flap Motion (k=0.04)

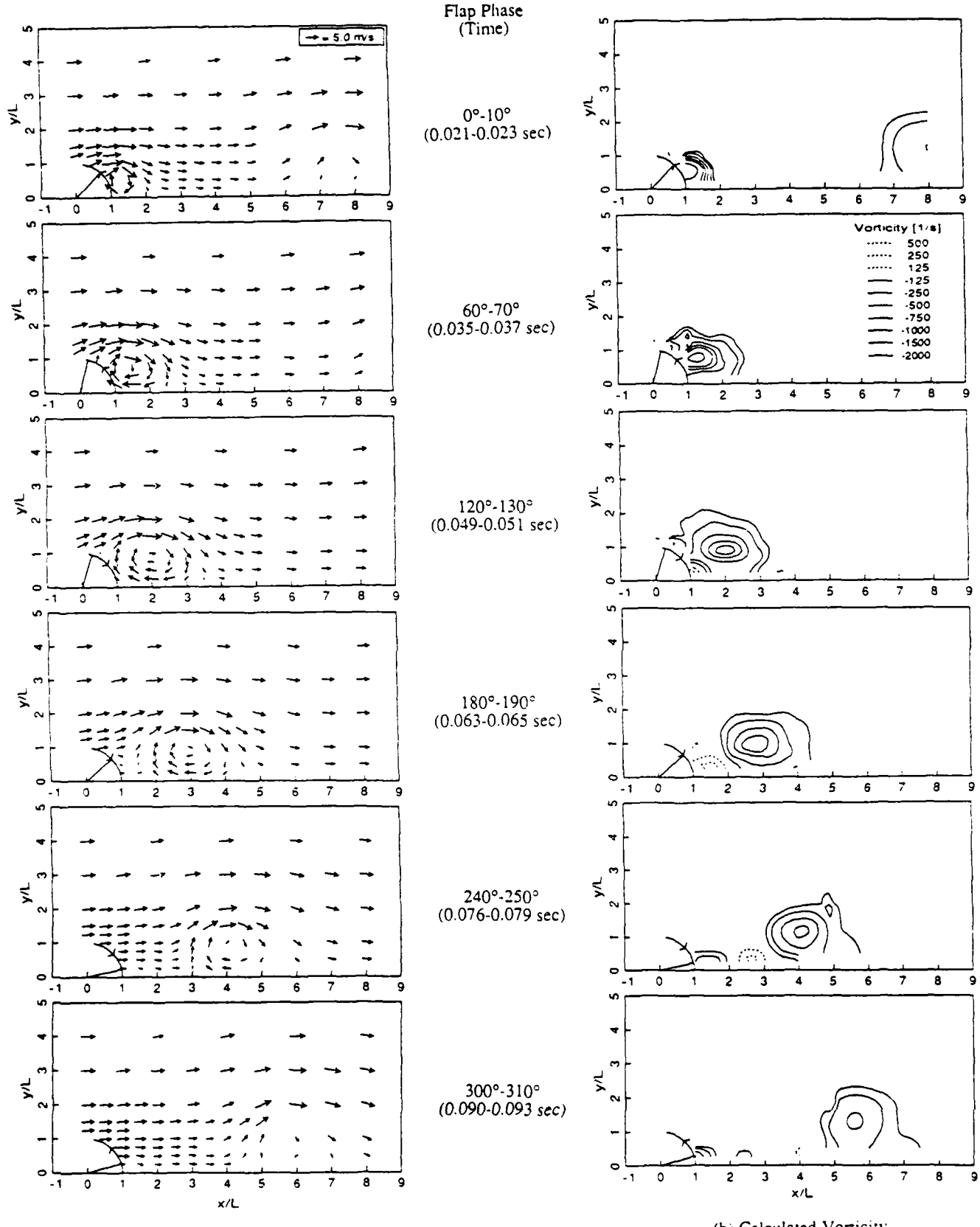

(a) Velocity Data

(b) Calculated Vorticity

FIGURE 5. Unsteady Flowfield for 12 Hz Sinusoidal Flap Motion (k=0.06)

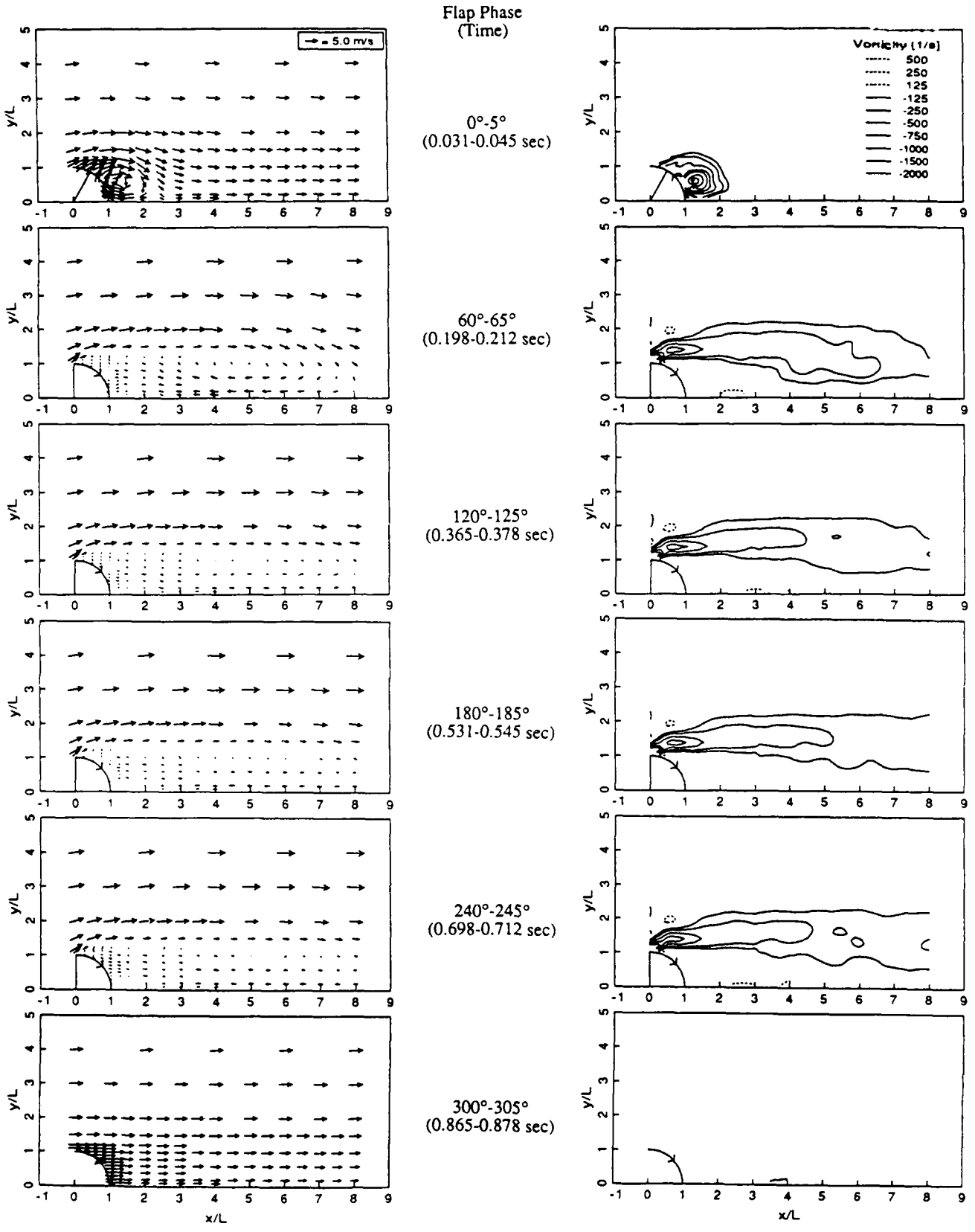

(a) Velocity Data

(b) Calculated Vorticity

FIGURE 6. Unsteady Flowfield for Pitch-and-Hold Flap Motion

vortex looks much like a quasi-steady separated region and a large shear layer is formed starting at the trailing edge of the flap. As the reduced frequency is increased, the size of this shear layer decreases and the unsteady vortex becomes more coherent. The presence of the strong, coherent vortex induces a region of secondary positive vorticity upstream of itself.

The pitch-and-hold waveform was investigated as a method of examining the unsteady vortex evolving into a steady separation. Figure 6 shows the velocity vectors and vorticity contours for this flowfield. As the flap rises, a strong unsteady vortex is formed, much like the 8 Hz sinusoidal case shown in Figure 4. However, since the flap holds when it reaches its maximum extension, the vortex is not cleanly carried away by the free-stream fluid. Instead a large separated region forms as boundary layer vorticity is carried over the flap by the mean flow. The vorticity contours in Figure 6 show the formation of a large shear layer at the trailing edge of the flap. The unsteady behavior of the vortex was examined in more detail using all 72 frames of the animated movie for this case. During the time in which the flap rises (φ=-11.25° to 11.25°) the flap motion and the flowfield are exactly the same as the k=0.04 sinusoidal case. When the flap holds at its maximum extension, the vortex begins to convect downstream while a shear layer forms at the flap trailing edge. By the 45°-50° phase bin, the vortex has convected out of the window of data, the flow behind the flap is stagnant, and a shear layer has formed from the flap trailing edge. However, in the range of phases from 50° to 65° the fluid near the wall in the separated region surges towards the flap and the shear layer dips toward the wall. The plot of the 60°-65° phase bin in Figure 6 shows the later stages of this surge. The flow then slowly adjusts until a steady separated region has been established by 120° phase . It should be noted that the "steady" separation contains large unsteadiness, but these velocity fluctuations are not phase correlated.

3.2. Unsteady Pressure

Figures 7 through 9 show the unsteady pressure measured on the bottom wall of the tunnel for the sinusoidal flap cycles corresponding to the velocity fields in Figures 3 through 5. In each case, the data show a well-defined negative pressure peak which convects downstream. This is a clear signature of the vortex observed in the detailed velocity measurements, suggesting that wall pressure data may be sufficient to track the vortices.

Pressure data for the pitch-and-hold flap motion is shown in Figure 10. An unsteady vortex is formed as the flap rises from the bottom wall of the tunnel, however as the vortex convects downstream a steady separated region is left behind, in agreement with the results shown in Figure 6. Note that the pressure overshoot which occurs between the large negative peak of the unsteady vortex and the flat region of the steady separation corresponds to the phase range in which the surge of backflow occurred.

3.3 Vortex Development

In order to quantify the development of the unsteady vortex during the flap cycle, the vorticity was integrated to calculate both the position and the circulation of the vortex as a function of flap phase for the sinusoidal flap motions. This was done by interpolating the velocity onto a fine mesh of points using the spline interpolation and calculating the vorticity for each of these points. The vorticity was integrated over all points in the field with negative vorticity of magnitude greater than 250 sec^{-1} to find the centroid and circulation of the vortex at each phase. The criterion of 250 sec^{-1} was chosen as it includes all the fluid which obviously belongs to the vortex, while excluding vorticity that might be background noise. The results for the k=0.04 and k=0.06 cases are plotted versus time in Figure 11, starting when the flap is flush with the tunnel bottom (*i.e.* starting at φ=270° for sinusoidal oscillations). The k=0.025 case is not shown as the flow was quasi-steady at this

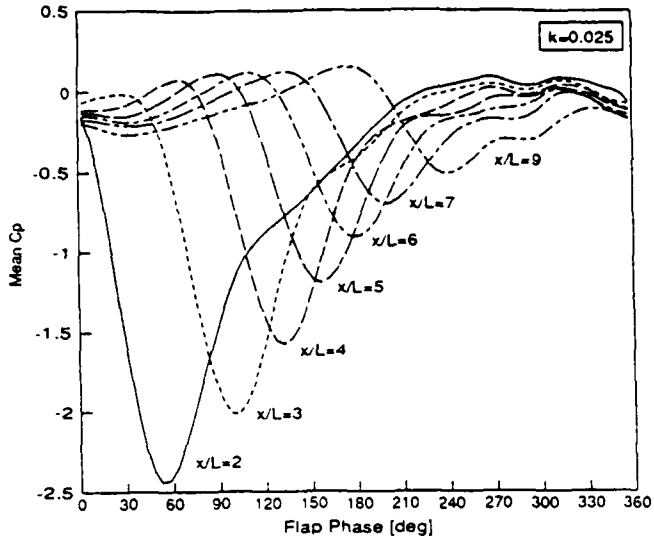

FIGURE 7 Unsteady Pressure for 5 Hz Sinusoidal Flap Motion

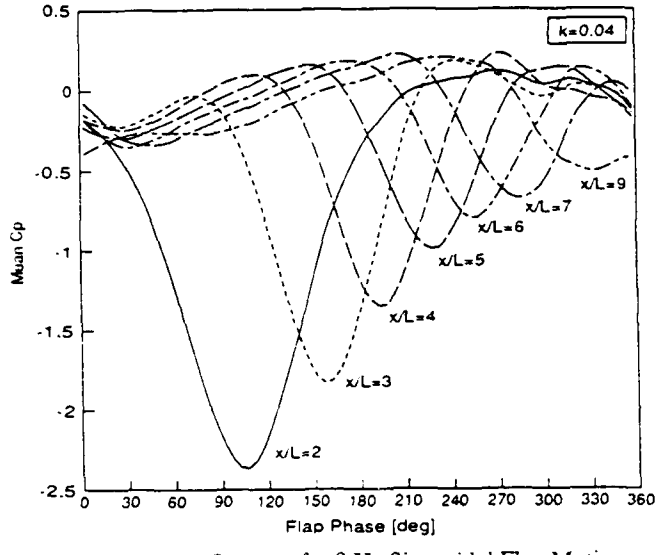

FIGURE 8. Unsteady Pressure for 8 Hz Sinusoidal Flap Motion

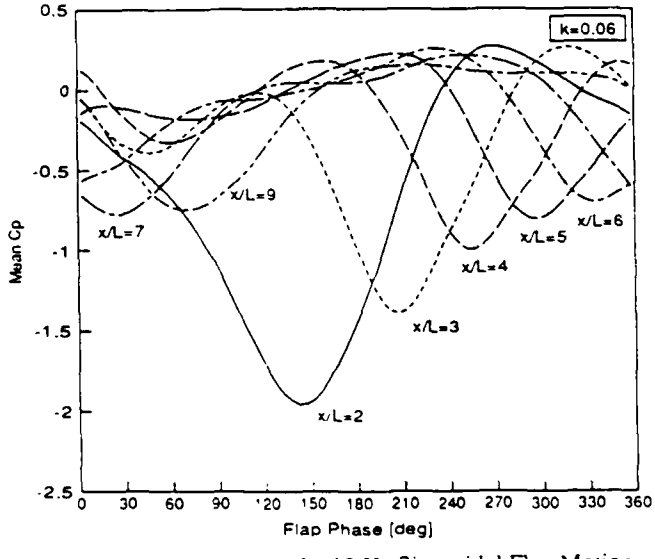

FIGURE 9. Unsteady Pressure for 12 Hz Sinusoidal Flap Motion

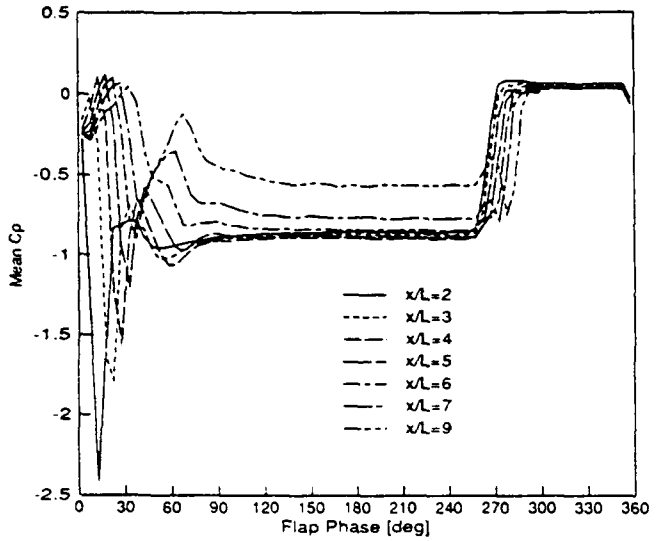

FIGURE 10. Unsteady Pressure for Pitch-and-Hold Flap Motion

low reduced frequency and a large separated region was formed, leaving no clearly defined vortex over which to integrate (see Figure 3).

Figure 11(a) shows the circulation contained in the vortex. The peak circulation is larger for the k=0.04 case since the slower flap motion allows more time for the boundary layer vorticity to be rolled-up into the vortex. However, due to the fact that there are more vortices formed per unit time for the k=0.06 case, the sum of the circulation in the vortices formed per unit time is approximately equal for the two cases. During the portion of the flap cycle in which the flap is moving away from the wall, the circulation in the vortex increases due to the influx of boundary layer vorticity flowing over the flap. Once the flap begins to move back towards the wall, the circulation decreases as the vortex convects downstream and vorticity diffuses out of the vortex. The circulation finally falls rapidly to zero as the vortex convects out of the window in which data was acquired.

From the slope of the curves in Figure 11(b), the vortex reaches a limiting velocity of about 60% of the free-stream velocity for both cases, however the vortex in the higher reduced frequency case is released from the flap at an earlier time due to the higher flap frequency. A simple explanation of why the vortex moves downstream slower than the free-stream velocity is the effect of the induced upstream motion on the vortex caused by its image vortex in the wall[13].

Figure 11(c) shows the height of the vortex centroid above the bottom tunnel wall. The vortex follows the sinusoidal motion of the flap to a height of y/L=1 and then remains at approximately the same height for the rest of the cycle. The curves become noisy at large time due to the fact that the vortices are beginning to flow out of the region where data was acquired and thus it becomes difficult to define where the center of the vortex is located.

3.4. Vorticity Transport

To take a closer look at the transport of vorticity in this flow, the vorticity fluxes have been calculated through control volumes located downstream of the flap. Utilizing tensor notation and the Cartesian coordinate system $(x,y,z) = (x_1,x_2,x_3)$, the vorticity equation for an incompressible Newtonian fluid of constant viscosity can be written as:

$$\frac{\partial \omega_i}{\partial t} + \frac{\partial (u_k \omega_i)}{\partial x_k} = \frac{\partial (\omega_k u_i)}{\partial x_k} + \nu \frac{\partial^2 \omega_i}{\partial x_k \partial x_k} \qquad (1)$$

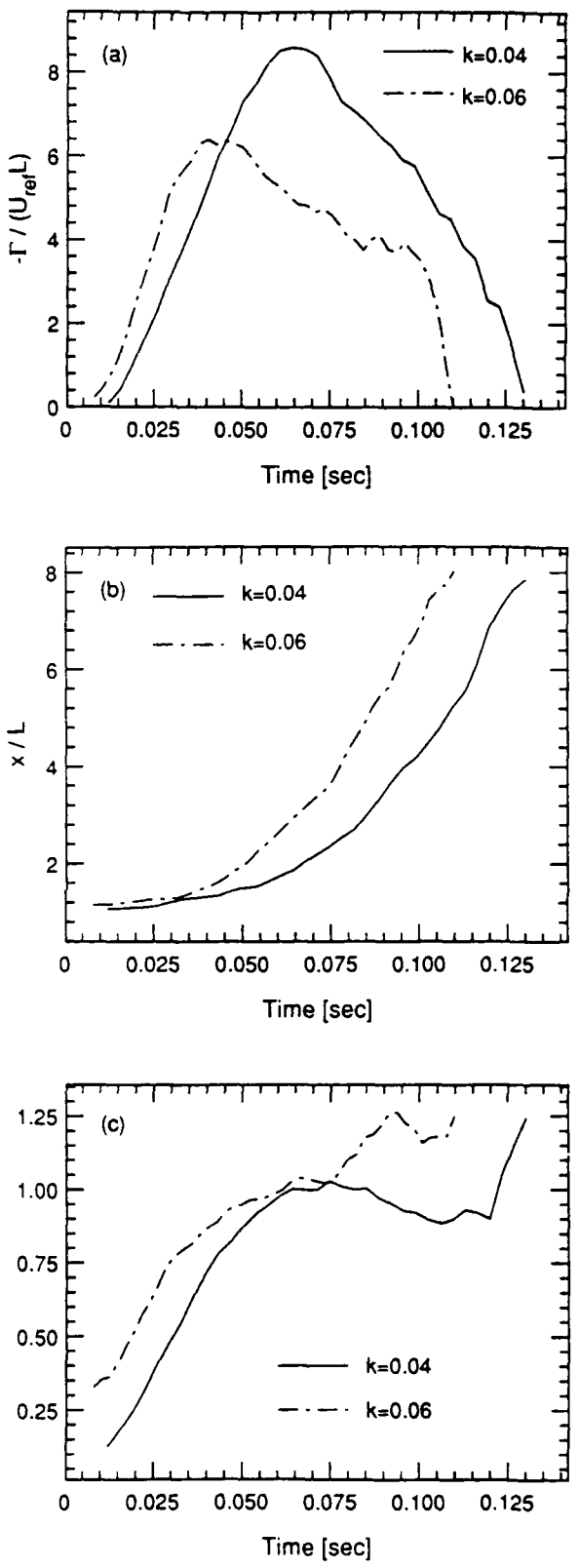

FIGURE 11. Unsteady Vortex Development
(a) Vortex Circulation
(b) Vortex Position Downstream
(c) Vortex Height

The time dependent velocity and vorticity terms can be decomposed into a phase-averaged mean term and a turbulent term. By phase-averaging the resulting equation, the mean vorticity transport equation becomes:

$$\frac{\partial \overline{\omega}_i}{\partial t} + \frac{\partial(\overline{u}_k \overline{\omega}_i)}{\partial x_k} + \frac{\partial(\overline{u'_k \omega'_i})}{\partial x_k} = \frac{\partial(\overline{\omega}_k \overline{u}_i)}{\partial x_k} + \frac{\partial(\overline{\omega'_k u'_i})}{\partial x_k} + \nu \frac{\partial^2 \overline{\omega}_i}{\partial x_k \partial x_k} \tag{2}$$

After assuming no gradients or mean flow in the spanwise direction ($\partial/\partial x_3=0$ and $\overline{u}_3=0$), the phase-averaged mean spanwise vorticity equation can be rewritten in flux form[13] as:

$$\frac{\partial \overline{\omega}_3}{\partial t} + \frac{\partial \overline{F}_k}{\partial x_k} = 0 \tag{3}$$

$$\overline{F}_k = \overline{u}_k \overline{\omega}_3 - \nu \frac{\partial \overline{\omega}_3}{\partial x_k} + \overline{\omega'_3 u'_k} - \overline{\omega'_k u'_3} \tag{4}$$

where F_1 and F_2 are the vorticity fluxes in the x- and y-directions. When the turbulent vorticity terms are expanded into derivatives of turbulent velocities, F_1 and F_2 are given by[14]:

$$\overline{F}_1 = \overline{u}_1 \overline{\omega}_3 - \nu \frac{\partial \overline{\omega}_3}{\partial x_1} + \frac{\partial}{\partial x_1}(\overline{u'_1 u'_2}) + \frac{\partial}{\partial x_2}\left(-\frac{\overline{u'_1 u'_1}}{2} + \frac{\overline{u'_2 u'_2}}{2} - \frac{\overline{u'_3 u'_3}}{2}\right) \tag{5}$$

$$\overline{F}_2 = \overline{u}_2 \overline{\omega}_3 - \nu \frac{\partial \overline{\omega}_3}{\partial x_2} + \frac{\partial}{\partial x_1}\left(-\frac{\overline{u'_1 u'_1}}{2} + \frac{\overline{u'_2 u'_2}}{2} - \frac{\overline{u'_3 u'_3}}{2}\right) - \frac{\partial}{\partial x_2}(\overline{u'_1 u'_2}) \tag{6}$$

The various terms in the fluxes represent vorticity transport by convection, viscous diffusion, shear-stress gradient, and normal-stress gradient. Note that under our assumptions of two-dimensional flow in the mean, there is no vorticity transport by means of vortex stretching. The normal-stress in the z-direction and the shear-stress terms were not measured, however some idea of their magnitude can be inferred by the amount by which this equation does not balance to zero. Experimental error and three-dimensional effects like vortex stretching will also contribute to the difference term.

In order to avoid using second derivatives of the acquired velocity data, the vorticity flux equation was integrated in space over a control volume in the flowfield. This integration was carried out for all four cases and the results are shown in Figures 12 through 15. The inset in each figure shows the control volume that was used, where each surface is shown in the same line style used to plot the flux for that surface. The vorticity flux in the positive coordinate direction (*i.e.* in the positive x- or y-direction) through each of the four surfaces defining the control volume is shown as a function of flap phase, with the net vorticity flux into the control volume plotted as a solid line. Note that the vorticity in this flow is negative and thus a flux in the positive coordinate direction will have a negative sign. The net flux should sum to zero over the entire cycle as this is equivalent to integrating the vorticity flux equation in time over a complete flap cycle. There can be no net increase or decrease of vorticity stored in the control volume over the entire cycle since the flow is periodic.

In all cases, there is a large flow of vorticity into the control volume through the upstream control volume surface

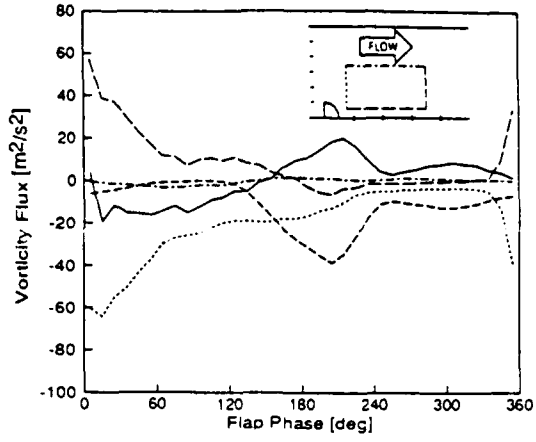

FIGURE 12. Unsteady Vorticity Flux for 5 Hz Sinusoidal Flap Motion (k=0.025)

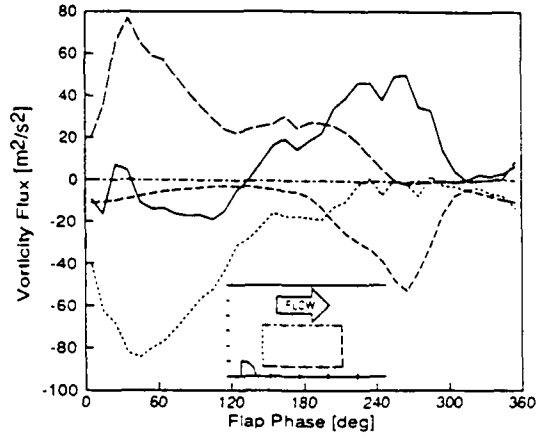

FIGURE 13. Unsteady Vorticity Flux for 8 Hz Sinusoidal Flap Motion (k=0.04)

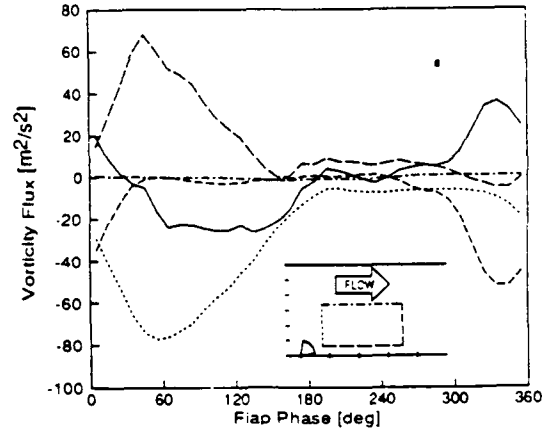

FIGURE 14. Unsteady Vorticity Flux for 12 Hz Sinusoid Flap Motion (k=0.06)

and a large flow of vorticity out the bottom surface for early flap phases (*i.e.* while the flap is rising). This is consistent with the fact that vorticity will be carried in through the upstream surface and out the bottom surface of the control volume as the vortex rolls-up behind the flap. During this part of the cycle, the net flux shows an overall inflow of vorticity since the vortex is growing into the control volume. When the vortex convects downstream its streamwise extent is entirely contained within the control volume and thus the fluxes

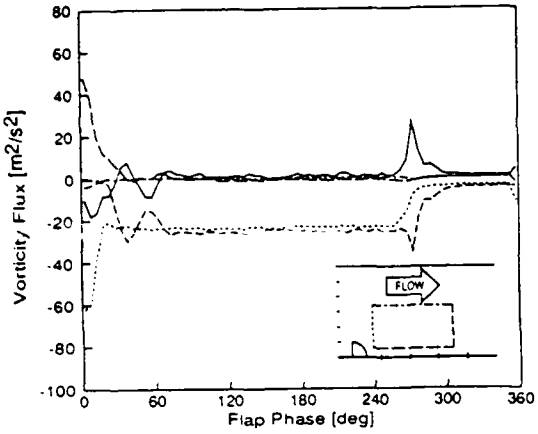

FIGURE 15. Unsteady Vorticity Flux for Pitch-and-Hold Flap Motion

through the upstream and downstream surfaces of the control volume are small. The flux through the bottom surface is also small as the upstream side of the vortex produces an inflow and its downstream edge produces an outflow of vorticity through the bottom surface which effectively cancel one another. When the vortex convects out the downstream surface of the control volume there is a large net outward flux of vorticity. The flux of vorticity out the upper surface of the control volume during the cycle is negligible as the surface was located well out in the free-stream. Because the vortex is much more coherent for the higher reduced frequency (k=0.06) case, the flux terms shown in Figure 14 are essentially zero for flap phases from 170° to 300° when the vortex is contained entirely within the control volume. The shear layers that are formed on the flap at the lower reduced frequencies keep the flux through the upstream surface of the control volume from going to zero, even when the unsteady vortex is entirely within the control volume. Comparison between Figures 3 to 5 and Figures 12 to 14 show excellent agreement as to when the vortex enters and leaves the control volume.

Figure 15 shows the same results for the pitch-and-hold case. Since a steady separation is formed, the vorticity flux into the upstream surface is equal to the flux out of the downstream surface for most of the cycle. A net change in the vorticity in the control volume occurs only when the flap is rising or falling. For example, from 254.25° to 276.75° phase the flap goes from being perpendicular to flush with the wall. The flux of vorticity into the upstream surface stops at about 280° phase and it stops flowing out of the downstream surface about 10° later in phase (=0.028 sec) which is essentially the time it takes for the free-stream to traverse the length of the control volume, carrying away the vortical fluid that was contained in the separated region.

The convective term is the dominant term in the vorticity transport equation. The viscous diffusion term and the measured normal-stress gradient terms are usually at least two orders of magnitude smaller. The sum of the net flux over the entire cycle for the k=0.04 sinusoidal case was equal to about 30% of the flux through the upstream surface of the control volume instead of summing to zero. However, for all the other cases the net flux summed to well under 5% of the flux through the upstream surface. The fact that the sum of the net flux over the cycle was so close to zero (aside from the k=0.04 case which may be an anomaly due to the effect of large changes in data spacing near the flap on the spline fit of vorticity) seems to indicate that the unmeasured terms in the vorticity transport equation are not very large. The fact that the fluxes are dominated by the convective term means that an inviscid, discrete-vortex model should give good results when modeling this flow. Note that even though the viscous and turbulent diffusion terms are negligible compared to the convective term for the overall transport of vorticity in this flow, these terms govern the growth of the vortex size and the time behavior of its peak vorticity.

4. CONCLUSIONS

Detailed phase-averaged measurement of unsteady velocity and pressure have been obtained in the unsteady, separated flow behind an oscillating flap. The phase-conditioned velocity measurements have provided quantitative estimates of vortex size, position, and strength in an unsteady separated flow. The vortex circulation decreases as the reduced frequency of the flap motion is increased, however the circulation per unit time remains relatively constant. For the range of reduced frequencies examined, convection of vorticity is the dominant term in the vorticity transport equation, while transport by turbulent stress gradients and viscous diffusion is several orders of magnitude smaller. These results indicate that inviscid models of this flowfield, such as discrete-vortex models, should be expected to work well in modeling this flow.

5. ACKNOWLEDGEMENT

This work is supported by the U.S. Air Force Office of Scientific Research Grant No. AFOSR-86-0159. The technical monitors are Capt. Henry Helin and Dr. James McMichael.

6. REFERENCES

[1] Francis, M.S., Keesee, J.E., *et al.*, "Aerodynamic Characteristics of an Unsteady Separated Flow," AIAA Journal, Vol. 17, No. 12, Dec. 1979, pp. 1332-1339.

[2] Consigny, H., Gravelle, A., and Molinaro, R., "Aerodynamic Characteristics of a Two-Dimensional Moving Spoiler in Subsonic and Transonic Flow," Journal of Aircraft, Vol. 21, No. 9, Sept. 1984, pp. 687-693.

[3] Costes, M., Gravelle, A., *et al.*, "Investigation of Unsteady Subsonic Spoiler and Flap Aerodynamics," Journal of Aircraft, Vol. 24, No. 9, Sept. 1987, pp. 629-637.

[4] Viets, H., Piatt, M., and Ball, M., "Forced Vortices Near a Wall," AIAA 19th Aerospace Sciences Meeting, AIAA-81-0256, Jan. 1981.

[5] Huyer, S.A. and Luttges, M.W., "Unsteady Separated Flows Driven By Periodic Leading Edge Deformation," AIAA 19th Fluid Dynamics, Plasma Dynamics and Lasers Conference, AIAA-87-1234, June 1987.

[6] Koga, D.J., "Control of Separated Flowfields Using Forced Unsteadiness," Ph.D. thesis, Illinois Institute of Technology, Dec. 1983.

[7] Reisenthel, P.H., Nagib, H.M., and Koga, D.J, "Control of Separated Flows Using Forced Unsteadiness," AIAA Shear Flow Control Conference, AIAA-85-0566, March 1985.

[8] Ahmed, S. and Hancock, G.J., "On The Local Flow About a Spoiler Undergoing Transient Motion at Subsonic Speeds," QMC/EP-1050, Queen Mary College, London, June 1983.

[9] Graham, J.M.R., private communication, 1987.

[10] Koga, D.J., Nelson, C.F., and Eaton, J.K., "A New Program for Active Control of Unsteady, Separated Flow Structures," Proceedings of the AFOSR Unsteady Separated Flow Workshop II, Colorado Springs, CO, July 1987.

[11] Adams, E.W. and Eaton, J.K., "An LDA Study of the Backward-Facing Step Flow, Including the Effects of Velocity Bias," Journal of Fluids Engineering, Vol. 110, No. 3, Sept. 1988, pp. 275-282.

[12] de Brederode, V.A.S.L. and Bradshaw, P., "Three-Dimensional Flow in Nominally Two-Dimensional Separation Bubbles. I. Flow behind a Rearward-Facing Step," I.C. Aero Report #72-19, Imperial College, London, 1972.

[13] Reynolds, W.C. and Carr, L.W., "Review of Unsteady,

Driven, Separated Flows," AIAA Shear Flow Control Conference, AIAA-85-0527, March 1985.

[14] Brereton, G.J. and Reynolds, W.C., "Experimental Study of the Fluid Mechanics of Unsteady Turbulent Boundary Layers," Thermosciences Division Report TF-29, Department of Mechanical Engineering, Stanford University, May 1987, pp. 213-215.

AIAA '89

AIAA 89-1027

Control of the Unsteady, Separated Flow Behind an Oscillating, Two-Dimensional Flap

C.F. Nelson, D.J. Koga and J.K. Eaton
Stanford University, Stanford, CA

AIAA 2nd Shear Flow Conference
March 13-16, 1989 / Tempe, AZ

Control of the Unsteady, Separated Flow Behind an Oscillating, Two-Dimensional Flap

Curtis F. Nelson*, Dennis J. Koga‡, John K. Eaton§

Department of Mechanical Engineering
Stanford University
Stanford, CA 94305-3030

ABSTRACT

Methods of passive and active open-loop control of the unsteady, separated flow produced downstream of a two-dimensional lifting flap have been examined. Phase-averaged, unsteady pressure measurements were used to measure the effect of the control on both the unsteady vortex formed as the flap lifts from the tunnel floor and the steady separation formed when the flap remains in the vertical position. The passive control experiments used two- and three-dimensional disturbances upstream of and at the separation line located at the trailing edge of the flap. Due to the fixed separation line of the flap, the unsteady vortex was not changed by the passive control, however significant increases were obtained in the pressure recovery for the steady separation. Using pulsed blowing and suction, the active control experiments were able to reduce the suction peak of the unsteady vortex by as much as 40% and delay the peak suction by 14 milliseconds in addition to increasing the pressure recovery in the steady separation. A simple model for estimating the x-position, y-position, and circulation of the unsteady vortex using the measured pressures shows good agreement with vortex properties calculated using detailed velocity measurements.

NOMENCLATURE

c_p	Pressure coefficient, $(P - P_{ref})/(\rho U_{ref}^2/2)$
f	Frequency of the flap oscillation cycle [Hz]
k	Reduced frequency, $k = fL/U_{ref}$
L	Flap chord length = 25.4 mm
P	Static pressure on the wind tunnel bottom wall
P_{ref}	Reference (free-stream) static pressure
U_{ref}	Reference (tunnel centerline) velocity = 5 m/s
x	Streamwise distance from the flap rotation axis
y	Vertical distance from the tunnel bottom wall
z	Spanwise distance from the tunnel centerline
ϑ	Flap rotation angle (see Figure 2)
ϕ	Phase in the oscillatory flap cycle: $\phi = 0°$ occurs at the point $\vartheta = 45°$ when the flap is rising from the wall (see Figure 2)

1. INTRODUCTION

The flow behind a two-dimensional, lifting flap serves as a simple model of more general unsteady, separated flows and also has practical application in its own right. It has been recognized that large vortical structures are the dominant feature in these flows and that the unsteady effects produced by these structures can be either beneficial or detrimental to overall device performance. For example, the initial flow structure which rolls-up behind the flap creates a strong spanwise vortex, a corresponding low pressure on the surface, and a substantial short-term lift augmentation. If the flap remains in the vertical position, a steady separation is formed as the vortex either sheds or decays, and the lift augmentation is lost as a stalled flow is formed. Coherent structures in the separated shear layer, though *not strong enough* to cause lift augmentation, can cause substantial buffeting. Understanding and manipulation of the unsteady flow structures would enable one to take advantage of the beneficial effects while mitigating the detrimental effects.

As summarized by Reynolds and Carr[1], the control or controlled generation of vortical structure is of utmost importance in experiments involving flow unsteadiness and separation control. This paper describes several attempts at controlling the unsteady flow behind a two-dimensional, lifting flap. The control mechanisms investigated are all open-loop control as there has been no attempt to measure variables in real-time and feed them back into the control algorithm.

In the context of this paper, passive control is defined as control which is always "on", *i.e.* the passive control is not time-dependent. Active control involves time dependence and actively adding or taking away energy from the flow.

The objective of the control in this paper is to change the strength and delay the formation of the unsteady vortex formed behind the flap in order to demonstrate that these unsteady structures can be controlled. A secondary objective is to change the "steady" separation (*i.e.* the reattachment length) formed when the flap remains perpendicular to the bottom wall of the

* Research Assistant, Student Member AIAA
‡ Senior Research Associate, Member AIAA
§ Associate Professor and Associate Chairman, Member AIAA

tunnel. Note that the "steady" separation actually contains large unsteadiness, but the velocity and pressure fluctuations are not phase-correlated.

2. EXPERIMENTAL TECHNIQUE

The experiments were performed in a low-speed, 150 mm × 450 mm, open-circuit wind tunnel used in earlier backward-facing step flow experiments[2]. The test section was modified to eliminate the step and install the flush-mounted flap. The approach flow is tripped on all four tunnel walls and the boundary layers are allowed to develop over a 3.5 m length. The side-wall boundary layers are removed approximately 27 flap lengths upstream of the flap to maintain a two-dimensional approach flow. At the nominal free-stream velocity of 5 m/s, the Reynolds number based on flap chord is 8200, and the boundary layer momentum thickness Reynolds number is 1900.

Data acquisition and processing were done on a Masscomp MC-5500 computer system. This computer is able to control the tunnel speed, command the flap motion, and actuate control devices while simultaneously acquiring the unsteady pressure data. Using a single computer eliminated synchronization problems that would occur if several computers were needed to accomplish these tasks.

2.1. OSCILLATING FLAP

The two-dimensional flap is located on the bottom wall of the tunnel and spans the test section as shown in Figure 1. The flap aspect ratio (span/chord) is 18 to ensure two-dimensionality of the separated region[3]. The flap is actuated by a computer-controlled servo system driving a printed-circuit motor directly connected to the flap shaft and is free to oscillate from a position flush with the bottom surface of the tunnel ($\theta = 0°$) to a position perpendicular to the bottom wall ($\theta = 90°$). The flap waveform is specified by loading appropriate position information into computer memory and sending the signal out through a digital-to-analog converter to the servo system. Flap position and velocity feedback are provided by a rotary variable differential transformer (RVDT) and tachometer both mounted directly to the flap shaft.

Figure 2 shows the relationship between flap angle and flap phase for the flap waveforms used in this experiment. In all cases, the range of flap motion is from 0° to 90°. The flap reduced frequency is rather low as the maximum speed of the flap trailing edge is only 20% of the free-steam speed for an 8 Hz sinusoidal flap oscillation (k = 0.04). The pitch-and-hold flap motion is actually a 1 Hz cycle that starts as though it were an 8 Hz sinusoid (effective k=0.04) except the flap holds for 0.675 seconds once it reaches its maximum extension from the tunnel floor. After the flap returns to the wall as an 8 Hz sinusoid, it remains flush with the bottom wall of the tunnel for 0.2 seconds in order for the flow to re-establish itself before the start of the next cycle. Note that a phase difference of 360° for an 8 Hz waveform corresponds to a 0.125 second time difference compared to 1.0 second for the 1 Hz pitch-and-hold waveform.

2.2. PRESSURE MEASUREMENT

Pressures were measured using a Validyne CD15 carrier/demodulator and a Validyne DP45-16 pressure transducer connected differentially between the tunnel floor and the free-stream static pressure. Typically, 144 data samples were acquired during each flap cycle (phase resolution of 2.5°) and phase-averaged over 400 flap cycles.

When measuring unsteady pressures, the tubing and transducer response characteristics influence the acquired data. The ideal solution is to mount the pressure sensor flush with the wall at the point where the pressure is to be measured, but this was not feasible for two reasons: (1) the differential pressures in this experiment are very small because of the low free-stream velocity (the free-stream dynamic pressure is only 0.06 inches of water), and (2) flush-mounted transducers, such as microphones, that can measure these low differential pressures are physically too large for the spatial resolution that is necessary (the flap length is only 1 inch and typical microphones are 1/2 inch in diameter). Thus, the unsteady pressures were measured using a pressure transducer connected to the tunnel with 0.125 inch diameter Tygon tubing.

To investigate the effects of the tubing, the frequency response of the pressure measurement system was measured relative to the response of a flush-mounted condenser microphone (B&K Type 4134) using the pressure waveform created by an audio speaker driven at known frequencies. The resulting frequency response is shown in Figure 3. Due to the fact that neither the microphone nor the audio speaker were capable of operating at frequencies lower than 4 Hz, we were unable to measure the response of the pressure system over the entire range of frequencies that are important in the data to be presented. For example the pitch-and-hold flap motion is actually a 1 Hz cycle, thus the response of the pressure system to a 1 Hz signal must be known in order to properly compensate for the non-ideal frequency response of the pressure measurement system. Because of this, the unsteady pressure data presented in this paper has not been corrected for the phase lag and gain of the pressure transducer-tubing system. Figure 3 shows that the lag in the system is

non-negligible at low frequencies, however the gain of the system is very flat from 4–20 Hz.

3. RESULTS AND DISCUSSION

The unsteady flowfield for the lifting flap has been previously documented by Nelson *et al.*[4] using phase-averaged laser-Doppler velocimetry. Figure 4 shows measured velocity and calculated vorticity values for an 8 Hz sinusoidal flap oscillation (k=0.04) and Figure 6 shows the corresponding unsteady pressures measured downstream of the flap. As the flap rises away from the wall, a strong vortex is formed and negative velocities with magnitudes larger than the free-stream velocity are observed. The vortex grows until the flap reaches its maximum extension away from the wall. When the flap begins to move back towards the wall, the vortex is released and convects downstream. The pressure data shows the distinctive negative peak in the differential pressure caused by the unsteady vortex. It is obvious from Figures 4 and 6 that the flowfield is dominated by the presence of the large, unsteady vortex.

Figures 5 and 7 (also from the previous reference) show the same type of results for the pitch-and-hold flap motion. As the flap rises from the wall, an unsteady vortex is formed just as in the 8 Hz sinusoidal case and the characteristic negative pressure peak is seen ($\phi \approx 0°-80°$). However when the flap holds at its maximum extension, the vortex convects downstream leaving a region of stagnant fluid and forming a shear layer from the flap trailing edge. After the unsteady vortex convects downstream, a period of readjustment occurs as seen by the pressure overshoot between the large negative pressure peak of the unsteady vortex and the constant pressure region of the steady separation ($\phi \approx 30°-90°$). The flow then reaches a steady separation in the phase- or time-averaged sense. In reality, vortex structures continue to be shed from the flap trailing edge, however they are not phase-correlated. At a flap phase of approximately 270°, the flap returns to the wall so another cycle of data can be acquired and the flow quickly adjusts back to a flat-wall boundary layer.

The values of time shown in Figures 4 and 5 start at t=0 when the flap is flush with the bottom wall of the tunnel and is just beginning to rise (*i.e.* at $\phi = 270°$ for the sinusoidal flap oscillations and $\phi = 348.75°$ for the pitch-and-hold motions).

Control results will be presented for the sinusoidal and pitch-and-hold flap motions at a reduced frequency of 0.04. Smoke-wire flow visualization shows that the flow structure in the separated region downstream of the oscillating flap is very repeatable from cycle-to-cycle, thus all measurements are conditioned on the phase of the flap motion. In all cases the nominal free-stream velocity is 5 m/s.

It must be emphasized that the flap is used to create the unsteady flow, and it is *not* used for the control. Other devices are used to control the unsteady flowfield produced by the oscillating flap.

3.1. PASSIVE CONTROL

All the passive control measurements were taken for pitch-and-hold flap motions. The pitch-and-hold flap motion allows the measurement of the unsteady vortex formed during the rising part of the flap cycle and its development into a steady separation when the flap holds in the vertical position.

The passive control experiments attempted to modify the formation of the vortical structures using two- and three-dimensional disturbances upstream of and at the flow separation point.

Passive control upstream of the separation line was implemented using static longitudinal vortex generators. In a previous experiment by Westphal *et al.*[5], longitudinal vortices produced by vortex generators upstream of separation increased the entrainment into the separated shear layer. Four vortex generators were placed in the wind tunnel as shown in Figure 8a so that the images of the vortex generators in the tunnel side-walls would effectively produce an infinite array of generators. The measured pressures downstream of the flap for the vortex generators are shown in Figure 9. The vortex generators have minimal effect on both the unsteady vortex formed when the flap is rising and the steady separation. Pressures were measured at spanwise locations two flap lengths apart to check that this result was not a function of where the measurements were taken with respect to the vortex generators. The vortex generators are ineffective because they cannot change the location of the separation line which is fixed at the trailing edge of the flap. The streamwise vortices produced by the vortex generators are also very weak when compared to the spanwise vortex produced by the flap.

In order to get some type of effective passive control, it was decided to implement the control at the separation line using both two-dimensional and three-dimensional disturbances. Two-dimensional disturbances at the separation line were produced by oscillating the flap at 40 Hz over an angle range of approximately 5° during the portion of the cycle when the flap is at its maximum extension. This was done in order to organize the structures in the shear layer that are formed from the trailing edge of the flap, as this has been shown to decrease the steady reattachment length in previous backward-facing step experiments[6]. Strictly speaking this is actually active control, however

the energy input is small and mainly serves to organize the existing structures rather than introducing substantial new vorticity. The measured pressures in Figure 10 show that the two-dimensional disturbance has only minor effects on the development of the initial unsteady vortex. However, it is apparent that the steady separation bubble is shortened as indicated by the increased pressure recovery obtained during the steady separation portion of the cycle.

Three-dimensional disturbances at the separation line were implemented using a flap with a notched trailing edge (shown in Figure 8b) in order to introduce curvature in the separation line. The kinking of the separation line introduces three-dimensionality into the shear layer formed at the flap trailing edge. This should cause changes in the transport of vorticity into and out of the separated region behind the flap. The measured pressures in Figure 10 show that the three-dimensional disturbance does indeed cause increased pressure recovery during the steady separation. This effect is much stronger than that caused by the two-dimensional disturbance for locations close to the flap during the steady separation, but is not as effective well downstream of the flap. The three-dimensional disturbance also has some effect on the unsteady vortex formation as the negative pressure peak is decreased in magnitude by a little over 20% and its width is reduced due to a slight delay in its initial development, however the peak itself is not delayed.

Summarizing the passive control experiments, the overall formation time and the strength of the unsteady vortex were not significantly altered. However significant decreases in the steady reattachment length were obtained.

3.2. ACTIVE CONTROL

The active control experiments utilized pulsed blowing/suction through an angled, spanwise slot located upstream of the flap as shown in Figure 8c. The exit of the blowing/suction slot (hereafter known simply as the blowing slot) spans the entire width of the tunnel and is located 3.5 flap lengths upstream of the flap rotation axis. The exit is angled at 45° in the upstream direction in order to increase the amount of boundary-layer fluid that is "collected" when the flow is exiting from the slot. As the circulation of the unsteady vortex comes from boundary layer vorticity flowing over the flap, changing the flux of boundary-layer vorticity using the blowing slot should cause some change in the unsteady vortex.

Periodic blowing and suction from the slot is produced by two 8-inch speakers driven by an audio amplifier. The control signal sent to the amplifier is output by the computer so the speaker waveform and the phasing between the blowing and the flap motion can be set to any desired value. Only sinusoidal speaker motions were used in the present experiment, thus the slot produces blowing during half the speaker cycle and suction during the other half cycle. An important parameter for the active control cases is the amount by which the speaker control signal lags the flap motion (as measured in degrees of flap phase). The lag is defined as the amount by which the zero phase point of the speaker control signal lags the point $\phi = 0°$ in the flap cycle. The zero phase point of the speaker control is the point at which the speaker control signal is zero Volts and the slot is producing blowing.

As an initial check on the effectiveness of the slot in controlling the flow, experiments were carried out using 8 Hz (k=0.04) sinusoidal flap oscillations with 8 Hz sinusoidal speaker motion. Figure 11 shows the effects of changing the phasing between the speaker pulsing and the flap motion. At the optimum phase lag of 275° between the speaker pulsing and the flap motion, phase delays of nearly 30° (0.010 sec) in the development of the negative pressure peak and a reduction of the magnitude of the peak by approximately 40% were obtained. The delay of 0.010 seconds is non-trivial since the free-stream fluid travels two flap lengths during this period of time. Thus the pulsed blowing is able to exert useful amounts of control on the unsteady vortex formed behind the flap.

For the speaker lag of 275°, the blowing cycle is initiated 85° (0.030 sec) before the start of the next flap cycle and the flap goes through another complete cycle before the disturbance caused by the blowing slot (at x/L=-3.5) arrives at the measurement location (at x/L=3). Thus there is a delay of 0.155 seconds (=0.030−0.125) before the control effect produced by the blowing slot reaches the measurement location. This corresponds to an average convection speed of the disturbance equal to 25% of the free-stream velocity.

Smoke-wire flow visualization shows that the most effective speaker-to-flap phase lag corresponds to the case where the stalled fluid produced by the blowing slot arrives at the flap as the flap is moving away from the wall. The region of stalled fluid surrounding the flap effectively "hides" the flap from the free-stream flow. Now the flow no longer separates as strongly from the trailing edge of the flap as the trailing edge is enveloped in stalled fluid caused by the blowing slot. This leads to the changes in the unsteady vortex seen in the measurements.

The effect of the speaker input power, and thus the amount of blowing, was also investigated. The results in Figure 12 show that the decrease in the magnitude

of the pressure peak and the delay in the unsteady vortex formation are smooth, monotonic functions of the speaker input power. For all the active control cases, the power sent to the speakers corresponds to the -36 dB curve.

The pulsed blowing slot was also used to control the flow produced by pitch-and-hold flap motions (effective k=0.04). In order to control the unsteady vortex formed during the 8 Hz rising portion of the flap cycle, a continuous 8 Hz speaker motion was used. Thus there are eight blowing/suction cycles during one flap oscillation since the pitch-and-hold flap motion occurs on a 1 Hz cycle. This means that speaker lags separated by integer multiples of 45°, for example 10° and 325°, are indistinguishable. The results shown in Figure 13 indicate that the optimum speaker lag is approximately 347° for which the negative pressure peak is delayed in phase by almost 4° (0.011 sec) and its magnitude is decreased by 30%. The optimum speaker lag of 347° leads to a convection time from the blowing slot to the measurement point of 0.161 seconds which corresponds well with the sinusoidal flap case above.

From Figure 13 it can also be seen that the 8 Hz disturbances caused by the blowing slot are amplified when a steady separation is present ($\phi \approx 30°-270°$) as compared to when a boundary layer is present ($\phi \approx 270°-360°$) over the measurement location. This indicates that the perturbations caused by the blowing are amplified much more by the shear layer present when the flap is vertical than by the boundary layer present when the flap is flush.

The large 8 Hz pressure fluctuations on the wall during the steady separation are undesirable because of the unsteady force they create. In order to minimize this effect, the speaker motion was changed to a single 8 Hz pulse followed by low amplitude 40 Hz speaker oscillations. The 8 Hz pulse is used to control the unsteady vortex formed as the flap rises, and the 40 Hz waveform is to increase the pressure recovery during the steady separation portion of the cycle, much like that obtained for the passive control using two-dimensional disturbances at the separation line.

Figure 14 shows the measured pressures obtained as a function of the phase lag of the speaker (where the start of the 8 Hz pulse is the zero phase point of the speaker control signal used in defining the phase lag). The optimum phase lag is found to be 307° which causes a phase delay in the peak of the unsteady vortex of 5° (0.014 sec) and a decrease of 25% in the magnitude of the negative pressure peak. The optimum speaker lag corresponds to a convection time of 0.147 seconds between the blowing slot and the measurement location which agrees well with the previous active control cases. Unlike the previous case, the amplitude of the 40 Hz pressure signal seems to be independent of whether a shear layer or boundary layer is present over the measurement point.

3.3. VORTEX SENSING

In order to implement closed-loop control of the oscillating flap flow, some method of sensing both the presence and properties of the unsteady vortex will be necessary. A simple empirical model was developed to estimate values of the vortex position and circulation using the unsteady pressure data. The model is loosely based on the potential flow produced by a point vortex over an infinite plate.

Utilizing pressure data acquired at locations downstream of the flap (11 points were used, ranging from x/L=1.5 to x/L=9, and a natural cubic spline was fit to the data to improve the spatial resolution), the streamwise position of the vortex was assumed to be at the location of the minimum pressure. By matching the model to the magnitude and width of the measured suction pressure peak, the circulation and position above the wall of the unsteady vortex were estimated.

As shown in Figure 15 for sinusoidal flap oscillations, the values calculated using this model agree quite well with the actual unsteady vortex properties calculated from detailed velocity measurements of this flow[4] The results are plotted versus time, starting when the flap is flush with the bottom wall of the tunnel and just beginning to rise (*i.e.* at $\phi = 270°$ for the sinusoidal flap oscillations). The effects of the lag in the pressure measurements, as described in §2.2, can be easily seen in these results. This same model can be used to sense the initial unsteady vortex formed during the pitch-and-hold flap motions.

4. CONCLUSIONS

Even though the gross features of the oscillating flap flow were not modified by the investigated methods of control (*i.e.* an unsteady vortex is still formed and it still develops into a steady separated region), the results obtained are promising. The methods of passive control were unable to exert control over the unsteady vortex, however they were effective in decreasing the steady reattachment length. The active control exerted useful control over both the unsteady and steady flow. The suction peak of the unsteady vortex was reduced up to 40% and delayed by as much as 14 milliseconds. Thus, useful amounts of control have been exhibited over an unsteady flow in which the separation line essentially cannot be moved.

The convection time delay between when the upstream control is produced and when its effect is felt

downstream is not a problem in the present experiment as the flap motions are periodic and known. However for the general case of unknown flap motions, another control device must be added downstream of the flap so that control can be started as soon as a sensor detects that a separation is occurring. This additional device, possibly another blowing slot, would be used to control the initial unsteady development of the separation while the upstream blowing would add to the control effort a convection time later.

Future work will involve combining the upstream pulsed blowing control with another control device in the region downstream of the flap. Then the simple sensing model can be used to feed information about the separated vortex back to these control devices in order to implement true closed-loop control of this flow.

5. ACKNOWLEDGEMENT

This work is supported by the U.S. Air Force Office of Scientific Research Grant No. AFOSR-86-0159.

6. REFERENCES

[1] Reynolds, W.C. and Carr, L.W., "Review of Unsteady, Driven, Separated Flows," AIAA Shear Flow Control Conference, Boulder, CO, AIAA-85-0527. March 1985.

[2] Adams, E.W. and Eaton, J.K., "An LDA Study of the Backward-Facing Step Flow, Including the Effects of Velocity Bias," Journal of Fluids Engineering, Vol. 110, No. 3, Sept. 1988, pp. 275–282.

[3] de Brederode, V.A.S.L. and Bradshaw, P., "Three-Dimensional Flow in Nominally Two-Dimensional Separation Bubbles. I. Flow Behind a Rearward-Facing Step," I.C. Aero Report #72-19, Imperial College, London, 1972.

[4] Nelson, C.F., Koga, D.J., and Eaton, J.K., "Unsteady, Separated Flow Behind An Oscillating, Two-Dimensional Flap," AIAA 27th Aerospace Sciences Meeting, Reno, NV, AIAA-89-0288, Jan. 1989.

[5] Westphal, R.V., Johnston, J.P., and Eaton, J.K., "Experimental Study of Flow Reattachment in a Single-Sided Sudden Expansion," NASA-CR-3765, Jan. 1984.

[6] Roos, F.W. and Kegelman, J.T., "Influence of Excitation on Coherent Structures in Reattaching Turbulent Shear Layers," AIAA 24th Aerospace Sciences Meeting, Reno, NV, AIAA-86-0112, Jan. 1986.

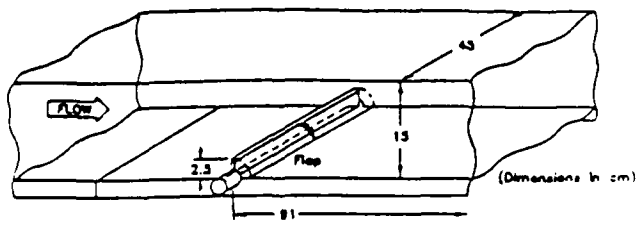

FIGURE 1. Schematic of Wind Tunnel Geometry

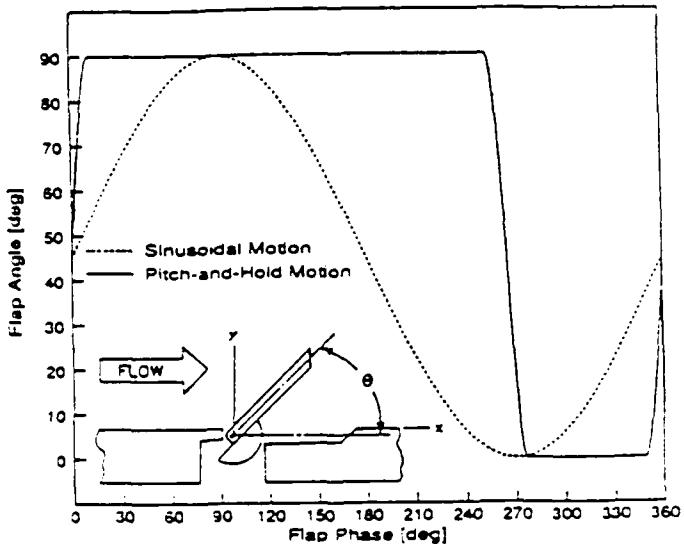

FIGURE 2. Flap Waveforms

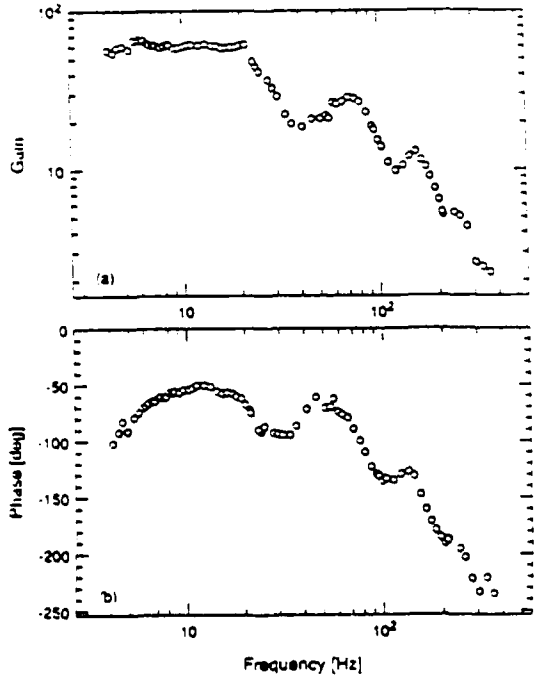

FIGURE 3. Frequency Response of Pressure Measurement System
(a) Gain
(b) Phase

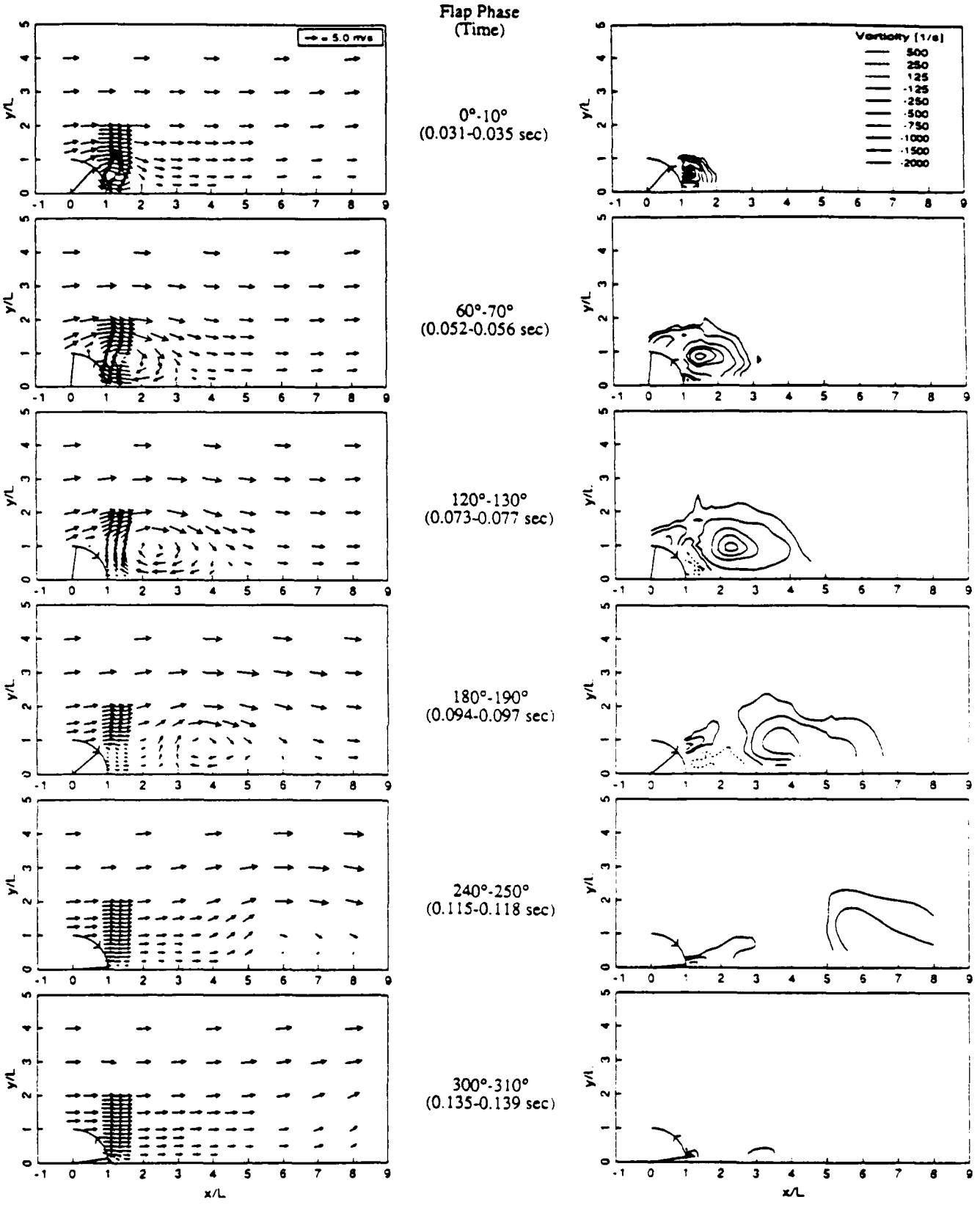

(a) Velocity Data

(b) Calculated Vorticity

FIGURE 4. Unsteady Flowfield for 8 Hz Sinusoidal Flap Motion (k=0.04)

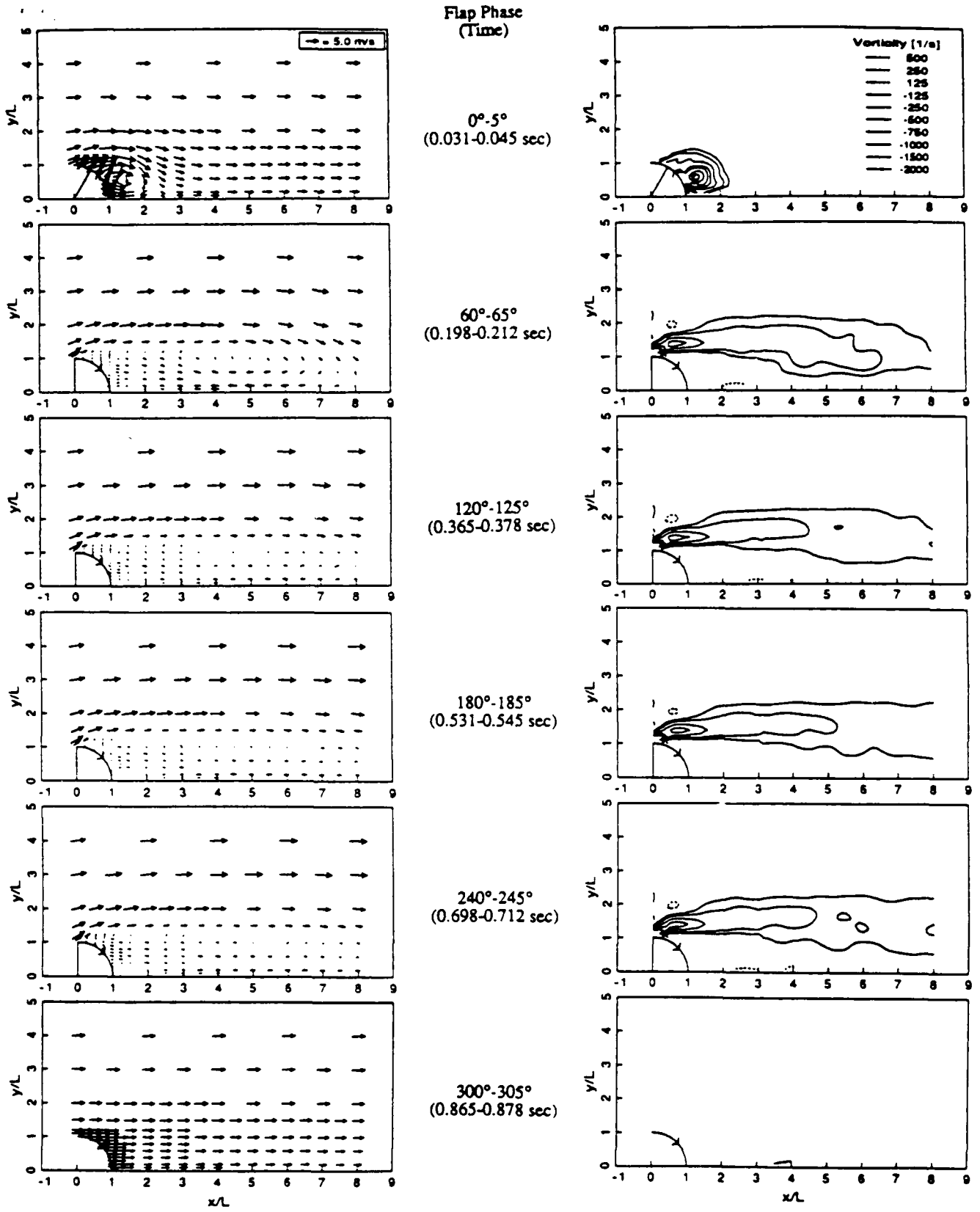

(a) Velocity Data

(b) Calculated Vorticity

FIGURE 5. Unsteady Flowfield for Pitch-and-Hold Flap Motion (effecuve k=0.04)

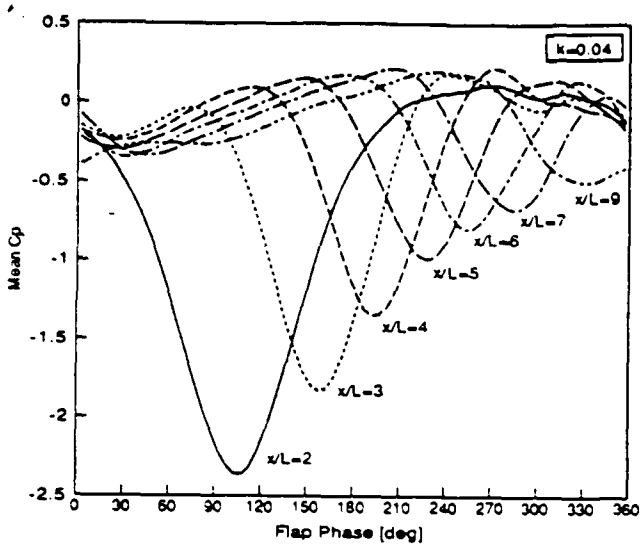

FIGURE 6. Unsteady Pressure for 8 Hz Sinusoidal Flap Motion

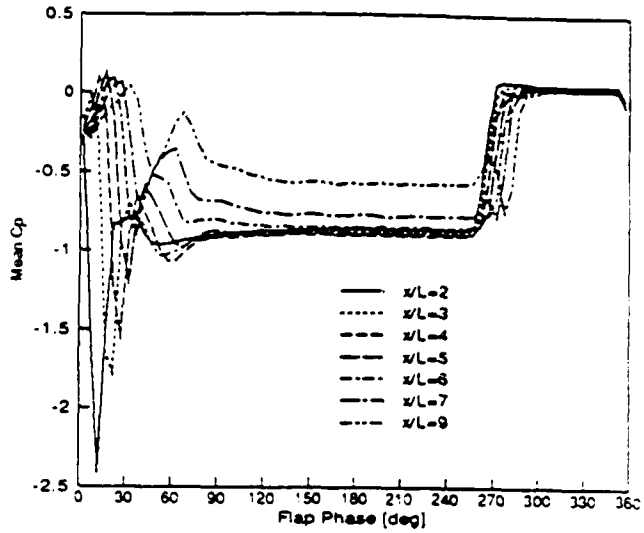

FIGURE 7. Unsteady Pressure for Pitch-and-Hold Flap Motion

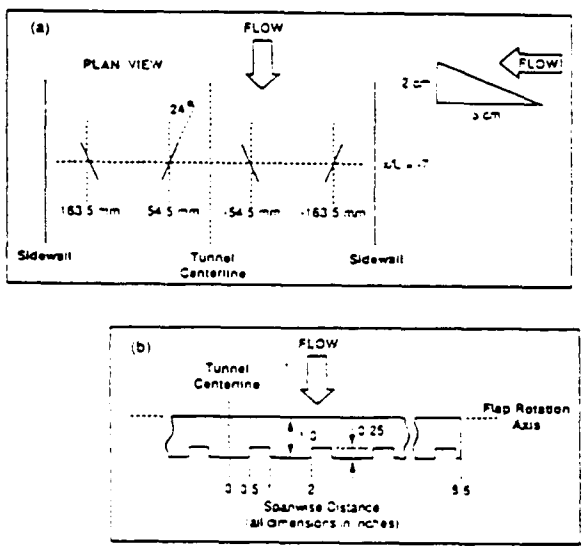

FIGURE 8. Schematics of Control Devices
(a) Vortex Generators for Passive Control
(b) Flap with Notched Trailing Edge for Passive Control
(c) Pulsed Blowing/Suction Slot for Active Control

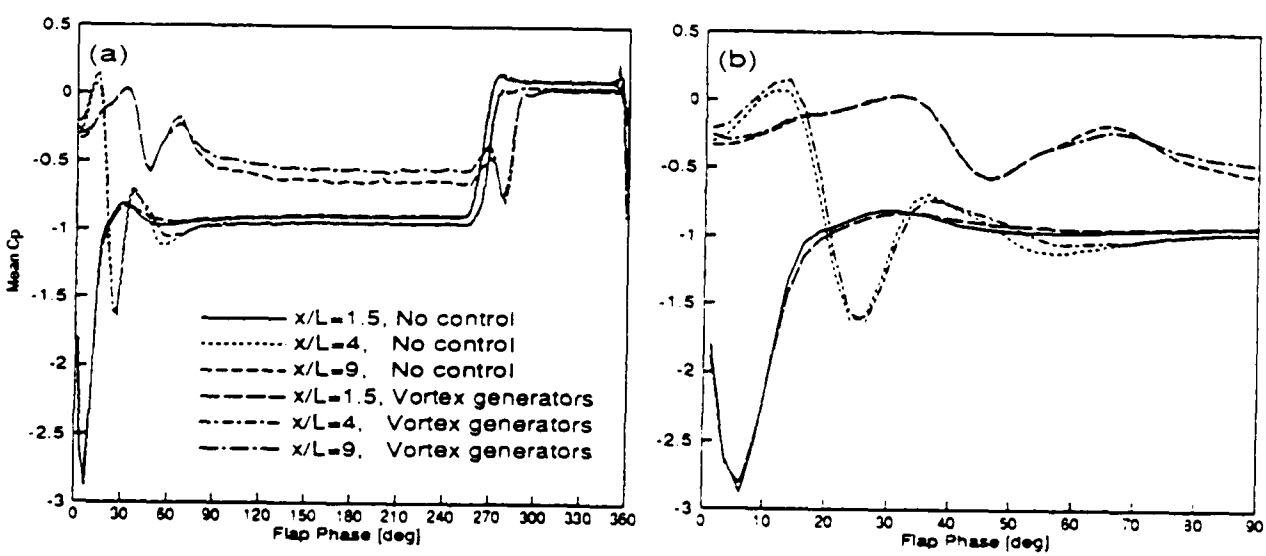

FIGURE 9. Passive Control of Pitch-and-Hold Flap Motion Using Vortex Generators
(a) Data for the entire cycle
(b) Detail of the initial unsteady vortex

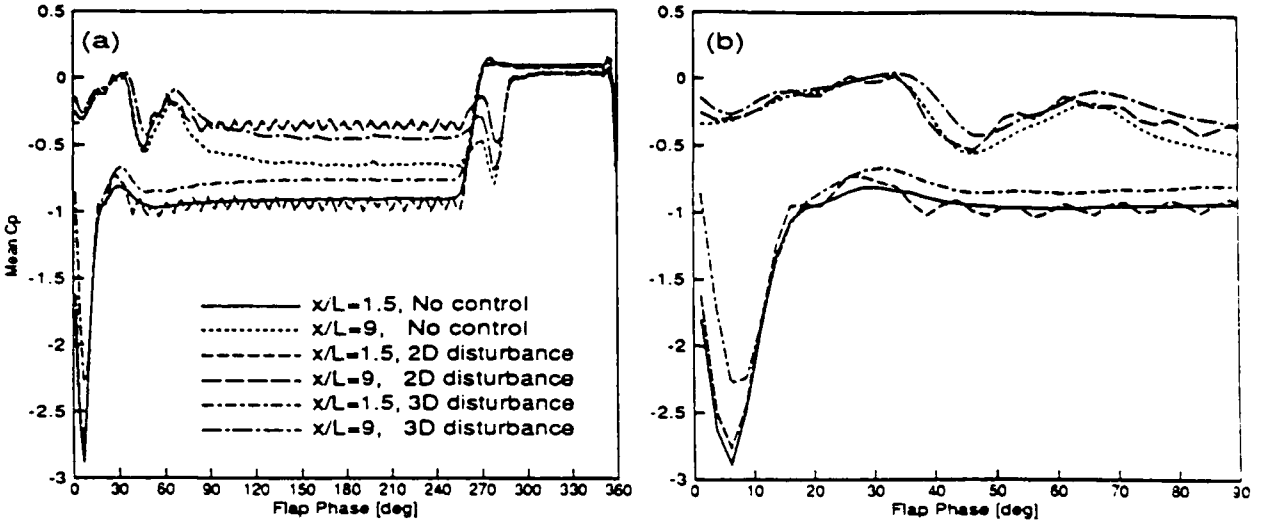

FIGURE 10. Passive Control of Pitch-and-Hold Flap Motion at Separation Line
(a) Data for the entire cycle
(b) Detail of the initial unsteady vortex

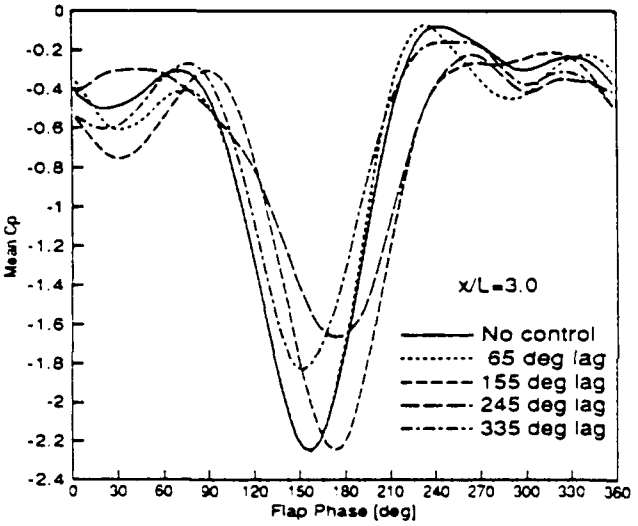

FIGURE 11. Effect of Active Control Phase Lag

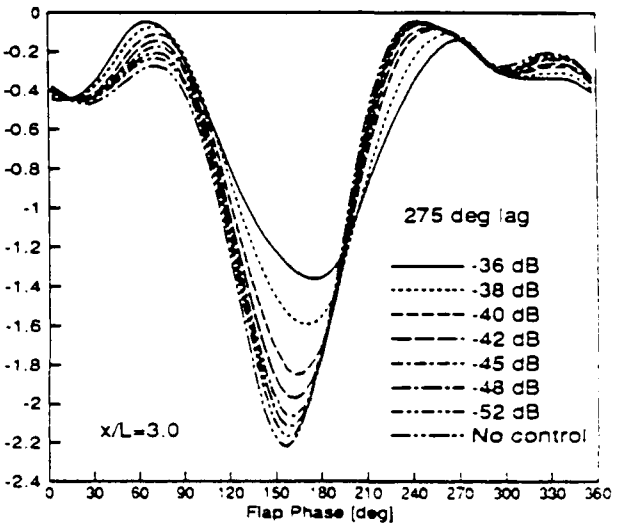

FIGURE 12. Effect of Active Control Power

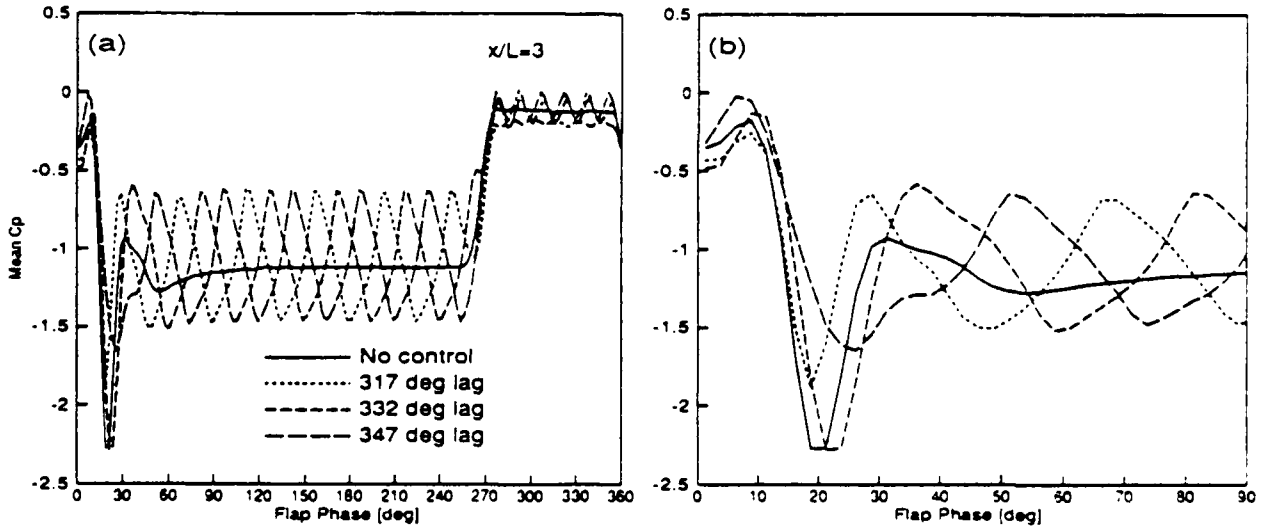

FIGURE 13. Active Control of Pitch-and-Hold Flap Motion Using 8 Hz Blowing
(a) Data for the entire cycle
(b) Detail of the initial unsteady vortex

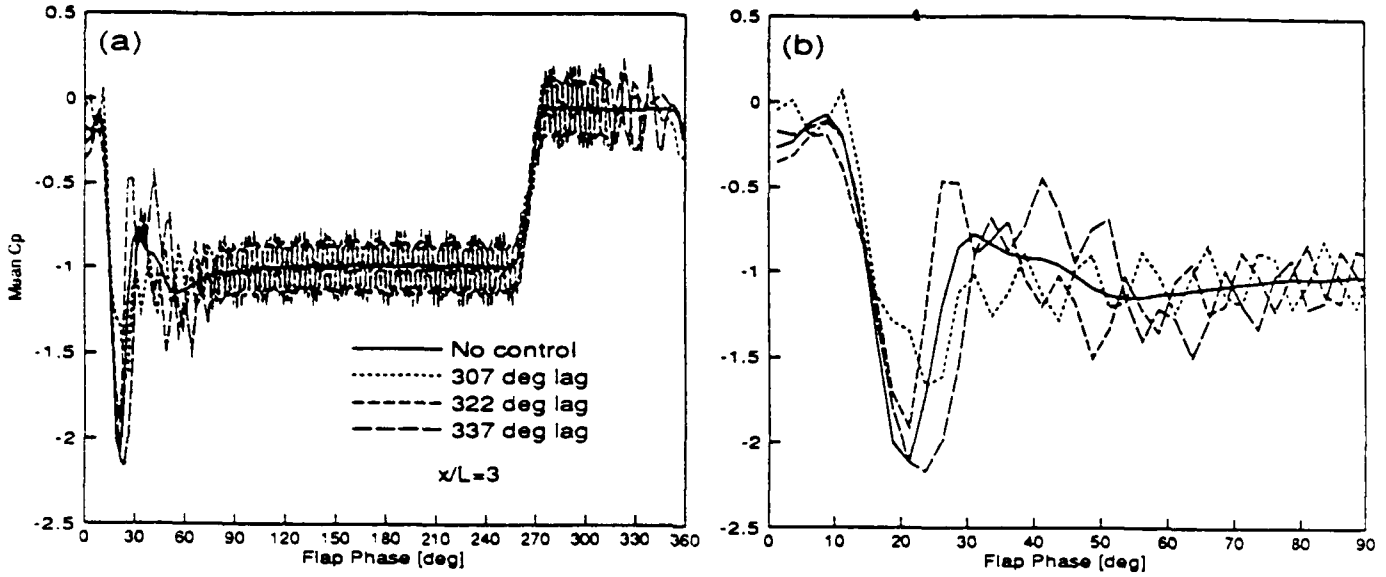

FIGURE 14. Active Control of Pitch-and-Hold Flap Motion Using 8 Hz/40 Hz Blowing
(a) Data for the entire cycle
(b) Detail of the initial unsteady vortex

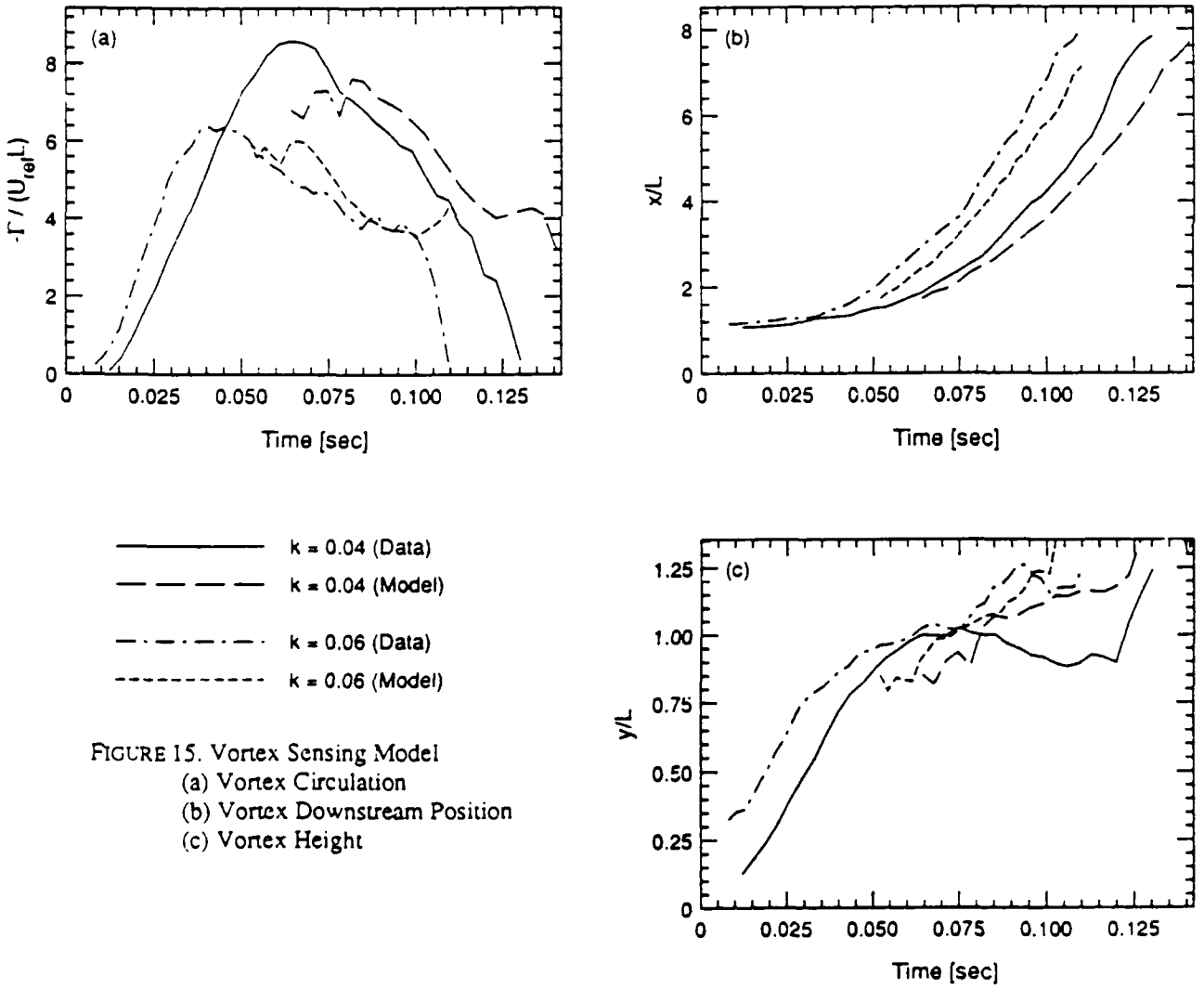

FIGURE 15. Vortex Sensing Model
(a) Vortex Circulation
(b) Vortex Downstream Position
(c) Vortex Height